Palaeogeography, Palaeoclimatology, Palaeoecology 640 (2024) 112085

Contents lists available at ScienceDirect

Palaeogeography, Palaeoclimatology, Palaeoecology

journal homepage: www.elsevier.com/locate/palaeo

The Cretan Basin (South Aegean Sea, NE Mediterranean) in the Early Pliocene: a paleoceanographic reconstruction

E. Skampa [a,*], M.D. Dimiza [a], A. Arabas [b], A. Gogou [c], I.P. Panagiotopoulos [a], Th. Tsourou [a], D. Velaoras [c], M. Karagiorgas [a], K.-H. Baumann [d], M.V. Triantaphyllou [a]

[a] National and Kapodistrian University of Athens, Faculty of Geology and Geoenvironment, Panepistimioupolis, 15784, Athens, Greece
[b] Institute of Geological Sciences, Polish Academy of Sciences, Research Centre in Kraków, ul. Senacka 1, Kraków, 31-002, Poland
[c] Hellenic Centre for Marine Research, Institute of Oceanography, P.O. Box 712, 19013 Anavyssos, Greece
[d] University of Bremen, Department of Geosciences, PO Box 33 04 40, 28334 Bremen, Germany

ARTICLE INFO

Editor: Howard Falcon-Lang

Keywords:
DSDP Site 378
Zanclean
South Aegean Sea
Calcareous Nannofossils
Paleoproductivity
Paleoenvironment

ABSTRACT

The Aegean Sea (NE Mediterranean) represents a key area for climatic and oceanographic future projections, therefore it is crucial to define its environmental evolution during the Pliocene paleoclimatic analogue. The DSDP Site 378, located in the South Aegean Cretan Basin, provides an exceptional opportunity to investigate in detail the paleoceanographic conditions of the Early Pliocene and to examine the basin's paleoenvironmental evolution, through the study of calcareous nannofossil accumulation rates and hydroclimate proxies. The sequence has been dated in between ~5.2–3.9 Ma, with the age of the first Zanclean marine sediments overlying the Messinian Primary Lower Gypsum demonstrating that the Cretan Basin was partially desiccated for at least ~400 kyrs, as a result of being a shallow epicontinental area in the Late Miocene. A relatively sudden change to deep marine environment took place in the Early Pliocene linked to the accelerated rate of trench extension in the Cretan Basin. The multi-proxy study revealed intervals reflecting warm surface waters and low-oxygen conditions on the seafloor, associated with the orbitally driven presence of Early Pliocene rhythmic sapropelic layers. Between ~5.2 and 4.6 Ma, the sapropelic layers were characterized by elevated abundance of *Reticulofenestra* spp. and *Florisphaera profunda,* depicting increased productivity throughout the photic zone. Both enhanced riverine inputs and weak presence of Levantine Intermediate Water (LIW) characterized this time interval. The alterations in the calcareous nannofossil patterns with increased *Helicosphaera* spp. and *Umbilicosphaera jafari* abundances, implying freshening and enhanced mid-photic productivity after ~4.6 Ma, suggest strengthening of LIW intrusion combined with the full restoration of North-South Aegean marine gateways that led to the establishment of a hydrographic system similar to the modern Aegean Sea.

1. Introduction

The Early Pliocene (5.3–3.6 Ma) represents one of the most puzzling intervals of long-term climatic evolution in the Cenozoic, characterized by weaker atmospheric circulation and deeper tropical thermocline (Fedorov et al., 2013). It is followed by the mid-Pliocene Warm Period (mPWP; 3.3–3.0 Ma), one of the best analogues for the present/future global climate change (Dowsett et al., 2016; Abell et al., 2021). Similarities between the mPWP and modern/future climate can be found due to comparable continental configurations, land elevations and ocean bathymetries (Dowsett et al., 2010). Although the origin of the Pliocene warmth is still on a debate, atmospheric and oceanic circulation driven climatic changes are widely suggested as a potential cause (e.g. Haywood et al., 2000; Haywood and Valdes, 2004). Similarly, the Mediterranean Sea, identified as one of the most responsive regions to global climate projections, is expected to become warmer and dryer by the end of the 21st century, consequently affecting the main mechanisms of the deep water formation and thermohaline circulation (IPCC scenarios; Ali et al., 2022, Mancini et al., 2023).

Prior to the warm Pliocene, the Late Miocene interval is marked by the Messinian Salinity Crisis (MSC) event in an isolated from the Atlantic Mediterranean Basin that caused the extensive deposition of thick and complex sequences of evaporites (e.g., Krijgsman et al., 1999; Roveri et al., 2014). The terminal phase of the MSC, is characterized by the

* Corresponding author.
E-mail address: elskampa@geol.uoa.gr (E. Skampa).

https://doi.org/10.1016/j.palaeo.2024.112085
Received 18 October 2023; Received in revised form 10 February 2024; Accepted 11 February 2024
Available online 13 February 2024

presence of brackish sediments, the well-known Lago-Mare oligo-mesohaline facies (e.g. Cita et al., 1990) with duration and environmental evolution still being controversial (e.g. Carnevale et al., 2006; Roveri et al., 2014; Andreetto et al., 2022). In particular, the documentation of planktonic foraminifera-rich layers (Spezzaferri et al., 1998; Iaccarino and Bossio, 1999), calcareous nannofossil assemblages (Spezzaferri et al., 1998; Corbí et al., 2016; Carnevale et al., 2019 and references therein), planktic diatoms (Pellegrino et al., 2021) and stenohaline marine fishes (Carnevale and Schwarzhans, 2022) in the Lago-Mare facies, provide solid evidence for normal marine environments, at least occasionally during the early stages of the Atlantic reconnection. In the same line, Roveri et al. (2008) suggest a stepwise base level rise possibly starting as early as 5.42 Ma, while more recently Mancini et al. (2022) and Pilade et al. (2023) confirmed the gradual return to marine conditions caused by one-way Atlantic inflow, already in the latest Messinian. In contrast, the catastrophic flooding scenario, being supported by seismic profiles and flood deposits (Garcia-Castellanos et al., 2009, 2020), corresponds to an "instantaneous" restoration of the marine setting (e.g., Iaccarino and Bossio, 1999; Caruso et al., 2020), induced by the collapse of the Gibraltar sill. The return to fully and stable marine conditions occurred with the Early Pliocene Mediterranean-Atlantic connection re-establishment after an event known as the Zanclean flood (Krijgsman et al., 1999; Blanc, 2002; Garcia-Castellanos et al., 2009). According to Garcia-Castellanos et al. (2009) the majority of the Atlantic water filled the entire Mediterranean within a time interval not exceeding two years. Interestingly, recent evidence (Amarathunga et al., 2022) suggest a recovery time of 26,000 years for the complete transition to normal marine conditions in the whole Mediterranean.

Apparently, the Mediterranean has become more sensitive to record the dominantly precession-induced climate oscillations since the East Antarctic Ice Sheet growth (Mourik et al., 2010). The combined effects of the axial and apsidal precession, resulting in an overall precession cycle of ~23 kyr on average, have led to the periodical deposition of several dark-coloured sapropelic layers (Rossignol-Strick, 1983; Hilgen, 1991), typically enriched in total organic carbon content (Kidd et al., 1978). Hence, sapropel deposition is continuously recorded in the eastern Mediterranean for the last ~15 Ma (e.g., Mourik et al., 2010; Athanasiou et al., 2017, 2021; Geraga et al., 2000, 2005; Grant et al., 2022; Triantaphyllou et al., 2009, 2016), related to changes in sea surface productivity, salinity and marine circulation in response to enhanced freshwater flux and subsequent organic matter preservation in the seabed during summer insolation maxima (e.g., Lourens et al., 1996; Rohling et al., 2015).

The Aegean Sea and particularly, the deep Cretan Basin in the South Aegean, are key areas for understanding past climate fluctuations, being important sources of deep water formation (DWF) and subsequent ventilation of the entire Eastern Mediterranean (e.g., Zervakis et al., 2004; Gačić et al., 2012; Velaoras et al., 2014). Indeed, the exchange of Ionian, Levantine and north-central Aegean water masses seas in the Cretan Basin, renders the area as a dynamic source of intermediate and, occasionally, deep water bodies (Velaoras et al., 2014). A major driving force for the climatic balance in the eastern Mediterranean is the formation of warm and saline Levantine Intermediate Water (LIW) that spreads westward at intermediate depths, preconditioning DWF during the winter months (e.g., Lascaratos et al., 1993; Velaoras et al., 2017). In addition, alterations of DWF areas between the Adriatic and Aegean Seas, similar to the Eastern Mediterranean Transient (EMT) event mechanism or other possible EMT-like phenomena, should be also expected to enhance the area's thermohaline circulation. Model projections have shown the Aegean to be the dominant source for the formation of eastern Mediterranean Deep Water at the first half of the 21st century, directly affected by the expected strengthening of the LIW (Parras-Berrocal et al., 2021, 2023).

The sedimentary record of DSDP Site 378, located in the north Cretan Basin of the South Aegean Sea, is so far the only available deep-water sequence from the South Aegean region that contacts at its base the primary facies of the Messinian evaporite formation (Hsü et al., 1978), similar to the typical onshore (e.g., Caltanissetta and Vena del Gesso basins in Italy, Sorbas basin in Spain; Lugli et al., 2010 and references therein) and offshore (Ochoa et al., 2015) Primary Lower Gypsum (PLG) deposits. This geoarchive is a unique record for the eastern Mediterranean, as PLG evaporites are found elsewhere in the Aegean and Ionian seas away from their major occurrence as isolated blocks (Karakitsios et al., 2013), while in Cyprus and the Levant margin they are documented within resedimented deposits (Lugli et al., 2013).

The analysis of the sediment record of Site 378 is promising for the creation of a high-resolution database for the environmentally sensitive area of the Cretan Sea, which will improve our knowledge of the response of the north-eastern Mediterranean during the warm early Pliocene and is expected to provide clues for deciphering the processes of the desiccated Cretan Basin. For this reason, calcareous nannofossils were studied, as they are not only an efficient biostratigraphic tool, but also ideal indices of paleoceanographic conditions due to their rapid response to environmental changes, primarily involving temperature, salinity, primary production and water stratification variations (e.g., Flores et al., 2005). In addition, the oxygen and carbon stable isotope compositions of planktonic foraminifera shells have been used as hydroclimate proxies (e.g., Mourik et al., 2010). Foraminiferal oxygen isotope composition ($\delta^{18}O$) provides an important indicator of the water temperature and salinity, with lower values indicating warmer and/or fresher conditions (e.g., Geraga et al., 2000; Lisiecki and Raymo, 2005), while the carbon isotope composition ($\delta^{13}C$) of planktonic foraminifera tests is widely used as an indicator of marine paleoproductivity (e.g., Geraga et al., 2005; Triantaphyllou et al., 2016; Athanasiou et al., 2021). The aforementioned proxies are combined with the results of elemental concentration and stable isotope measurements in order to document the productivity and organic matter preservation in respect to changes in basin ventilation (e.g., Arnaboldi and Meyers, 2006; Rohling et al., 2015). Therefore, the organic carbon and nitrogen isotope values ($\delta^{13}C_{org}$, $\delta^{15}N$) can provide important information on paleoproductivity changes as well as palaeoredox conditions (e.g., Arnaboldi and Meyers, 2006; Higgins et al., 2010; Möbius et al., 2010; Rohling et al., 2015), and organic matter origin and fate (terrestrial vs. marine, preservation vs. degradation processes, e.g., Nijenhuis and De Lange, 2000; Lamb et al., 2006; Triantaphyllou et al., 2016; Chaikalis et al., 2021).

Hence, the present study aims to: (a) establish a biostratigraphic framework and sound chronology for the Site 378 South Aegean record; (b) apply a multi-proxy approach to decipher the prevailing paleoceanographic conditions; (c) provide hints for the paleoenvironmental evolution of the Cretan Basin during the Early Pliocene.

2. Geological and oceanographic setting

The Aegean Sea consists of several inter-connected basins. In the South Aegean, between the Crete Island and Cyclades plateau, the studied Cretan Basin (Fig. 1) is located in the Neogene back-arc setting of the Hellenic Arc and trench system. Based on the relation between crustal thickness and extension, the models of previous studies (Jolivet et al., 1996) suggested that Crete is detached from the Cyclades area, with the main extensional phase of the Cretan Basin occurring between Late Miocene and Pliocene (Mascle and Martin, 1990; Papanikolaou and Vassilakis, 2010). According to the available paleogeographical interpretations (e.g., Roveri et al., 2014; Krijgsman et al., 2020; Andreetto et al., 2021) the South Aegean Sea, including the Cretan Basin was an almost, if not completely, isolated area during the late Messinian. In the same time, the North Aegean formed a semi-isolated brackish waterbody restricted by the Cyclades sill to the south, named "Egemar", with mixed influences from both Paratethys and Mediterranean water environments (Krijgsman et al., 2020).

The South Aegean, a "typical oceanic margin" environment, has minimal export rates of organic matter from the euphotic zone (mean

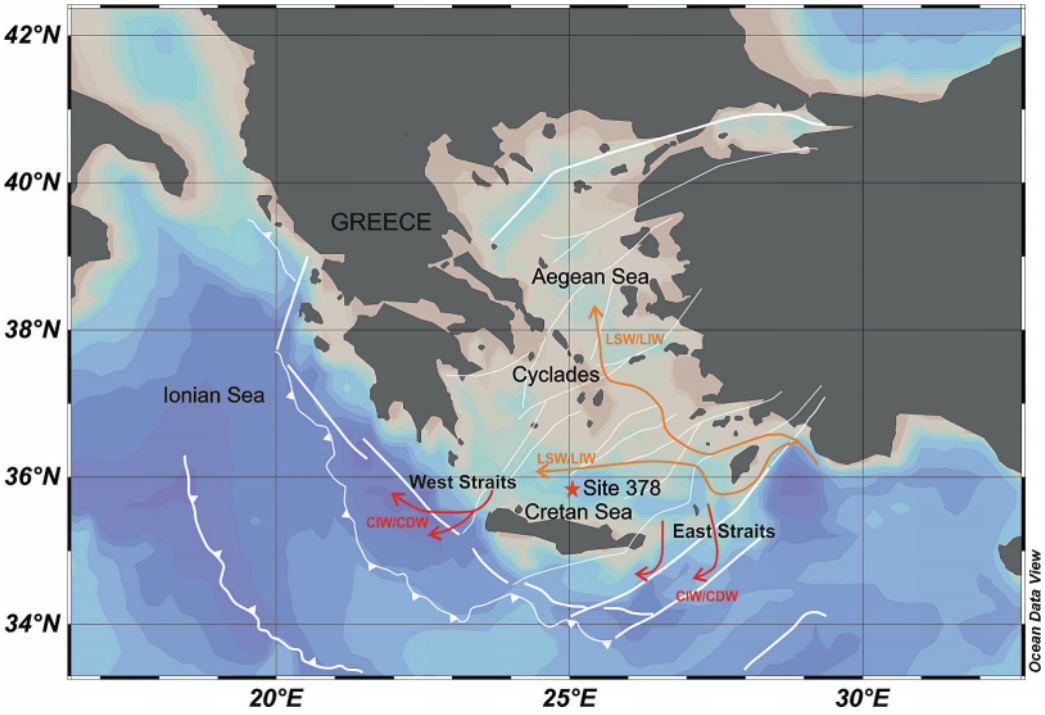

Fig. 1. Map of the major geodynamic elements [white lines modified after Tsampouraki-Kraounaki et al., 2021] of the Aegean Sea, colors related to sea bathymetry. Red Star: Leg 42A DSDP Site 378. Schematic representation of main water pathways in the Cretan Sea (LIW: Levantine Intermediate Water; LSW: Levantine Surface Water; CIW: Cretan Intermediate Water; CDW: Cretan Deep Water) after Velaoras et al. (2014). (For interpretation of the references to colour in this figure legend, the reader is referred to the web version of this article.)

annual flux at 200 m is 5.6 mg m^{-2} d^{-1}; Stavrakakis et al., 2000) and is covered by sediments with low organic matter contents (mean total organic carbon is 0.34%; Lykousis et al., 2002). The Cretan Sea (Fig. 1), the largest and deepest basin of the South Aegean (e.g., Georgopoulos et al., 2000), is connected to the east with the Levantine Basin through the East (Rhodes – Karpathos – Kasos) Straits and to the west with the Ionian Sea through the West (Kythira – Antikythira) Straits. One of the most important water bodies of the upper water column in the Cretan Basin modern hydrographic regime is the warm and highly saline (>39.3) Levantine Surface Water down to ~50 m depth) (Velaoras and Lascaratos, 2010). The warm Levantine Intermediate Water (LIW), with salinities ranging between 38.9 and 39.1 (Velaoras et al., 2014), occurs at 100–400 m depth (Lykousis et al., 2002), while the oxygenated Cretan Deep Water, with a salinity of up to ~39.08 (Velaoras et al., 2014), represents the deepest water mass in the Cretan Basin (below1000 m depth). Dense Aegean intermediate water masses that outflow from the Cretan Straits, form a discrete water mass known as dense Cretan Intermediate Water.

The ultra-oligotrophic Cretan Sea waters are characterized by the persistence of low concentrations of nutrients, low primary productivity values and phytoplankton densities, and the formation of a pronounced deep chlorophyll maximum (DCM; at 75–100 m depth) throughout most of the year (Psarra et al., 2000). Based on satellite measurements, surface Chl-a concentrations present maximum values during winter-early spring, coinciding with the sea surface temperature (SST) minima and precipitation maxima, as reported in Skampa et al. (2020).

3. Material and methods

DSDP Site 378 (Holes 378 and 378A; see Figs.1, 2) was drilled during Leg 42A on the northern flank a small depression in the north Cretan Basin (35°55.67′N, 25°06.97′E), at 1845 m water depth (Fig. 1; Table 1). The sequence is continuous with only one unconformity identified via seismic profiling within the Quaternary deposits (Hsü et al., 1978). Drilling commenced with Hole 378, but operational problems resulted in a number of non-fully recovered cores, e.g., in cores 9Z and 10Z (Hsü et al., 1978). Therefore, a final sampling effort was carried out to recover a deeper core, i.e. core 11Z. Hole 378 was terminated when the bottom of core 11Z came into contact with a caliche-like limestone identified in the core catcher, above the PLG selenitic gypsum, thus, supporting the uninterrupted recovery of the marlstone sequence. Even though the recovery of core 11Z was reduced by ~50%, this cannot introduce any bias into the interpretations provided by the current study, since our investigation focuses only on the retrieved uninterrupted core 11Z. A second hole, i.e., Hole 378A, was decided to drill at the same site in order to achieve some of the missed targets (see Hsü et al., 1978). Nevertheless, marlstones and Pliocene sapropels in Hole 378A were found as artificially emplaced on top of the recovered Miocene gypsum, by an abrupt contact caused by a drilling artifact (top of Core 4A; see Hsü et al., 1978). Both drilling holes (i.e., 378 and 378A) contain Early Pliocene sediments consisting of rhythmic alternations of calcareous nannofossil marlstone, ooze and sapropelic interlayers (Fig. 2, Hsü et al., 1978). Pre-Pliocene (Messinian) fossiliferous sediments were not recovered in Holes 378 and 378A; however, a sample processed from the gypsum lodged in the drill bit contained two individual fossil tests of planktonic (*Globigerinoides trilobus, G. obliguus extremus*) and one of benthic (*Bulimina* sp.) foraminifera, and one fragment of echinoid spine (Hsü et al., 1978), implying some evidence of marine origin.

For the objectives of the present study, a total of 279 samples from both Hole 378A (core 3A) and Hole 378 (core 11Z) were studied between 293.0 and 302.5 and 305.4–309.8 meters depth below sea floor (mbsf) respectively, assigned to the Early Pliocene interval (Hsü et al., 1978; Müller, 1978). The sampling resolution was about every 5–10 cm in the marly layers and every 1–2 cm in the sapropelic intercalations.

3.1. Elemental content, $\delta^{13}C_{org}$ and $\delta^{15}N$ of sediment samples

The sediment samples were treated with HCl (3N) and left overnight on a water bath at 60 °C under the lid. The carbonate-free residues were washed and rinsed several times with deionised water, oven-dried and,

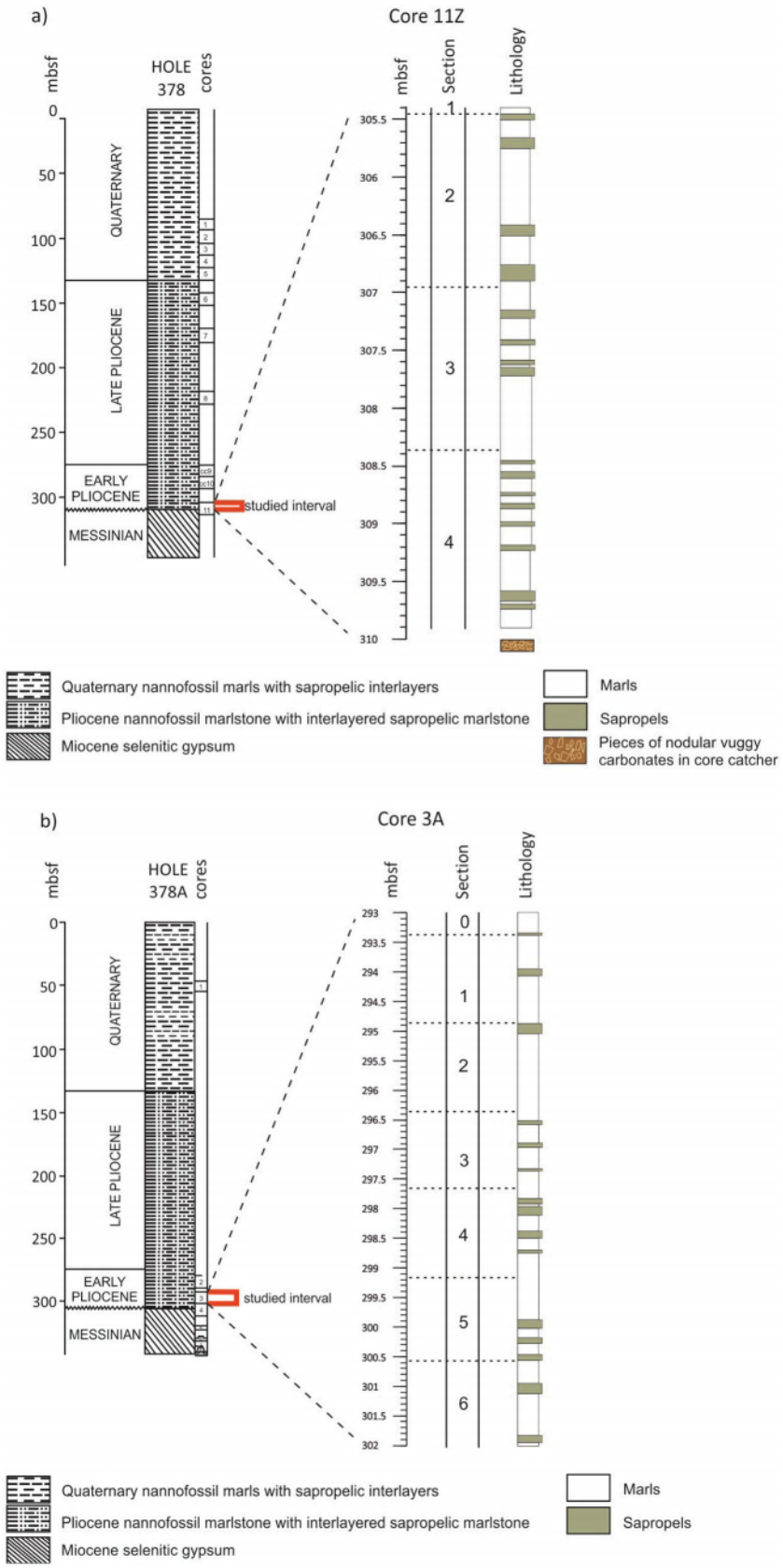

Fig. 2. Generalized lithology summary in Holes 378 and 378A, DSDP Site 378 according to Hsü et al. (1978) (a) Hole 378, Core 11Z, (b) Hole 378A, Core 3A.

Table 1
Coring summary according to the initial reports of the DSDP, Leg 42A (Hsü et al., 1978).

Hole	Core	Sections	Date	Time	Depth from Drill Floor (m)	Depth Below Sea Floor (m)	Cored (m)	Recovered (m)	Recovery (%)
378(Z)	11Z	1–4	18/5/1975	0955	2152.5–2157.0	305.4–309.8	9.5	4.7	49
378A	3A	0–6	18/5/1975	1655	2138.0–2147.5	293.0–302.5	9.5	9.5	100

*Coordinates of Site 378: 35°55.67′N, 25°06.97′E.

subsequently, grounded in an agate mortar. One hundred twenty-five samples were processed for measurements of the TOC content, carried out at the Institute of Geological Sciences of Polish Academy of Sciences in Warsaw, using a Vario MicroCUBE elemental analyser. The determination of the C_{org} and N isotope compositions ($\delta^{13}C_{org}$, $\delta^{15}N$) of the examined samples was conducted using a Thermo Flash EA 1112HT elemental analyser connected to a Thermo Delta V Advantage isotope ratio mass spectrometer. Isotope ratios are reported as delta (δ) values and expressed relative to the Vienna Pee Dee Belemnite (VPDB) international standard for $\delta^{13}C_{org}$ and atmospheric N for $\delta^{15}N$. Delta values have been normalized to a calibration curve based on the international standards USGS 40, USGS 41 and IAEA 600. The reproducibility of the relevant determinations was 0.06‰ and 0.13‰ (±1 s.d.) for the $\delta^{13}C_{org}$ and $\delta^{15}N$ values, respectively.

3.2. Foraminiferal analysis

For the analysis of the planktonic foraminifera, ~3 g of sediment material from each sample examined (63 samples in total), were soaked in hydrogen peroxide solution (50%), ultra-sonicated, and sieved u*sing* a stainless steel *sieve. The 63 and 125* μm fraction were both inspected, without showing significant compositional change, similar to the previous findings in other Mediterranean sites (Capotondi et al., 2002). Therefore, we used the 125 μm fraction, from which, we could obtain a more realistic spectrum of the assemblage (Capotondi et al., 2002), within the standard number of 300 individuals. For the identification of bioevents, the planktonic foraminifera assemblages were qualitatively scanned to determine the exact position of *Globorotalia margaritae* First Common Occurrence (FCO), *G. margaritae* Last Common Occurrence (LCO), and *Globoconella puncticulata* First Occurrence (FO) (Lirer et al., 2019; see detailed description in section 5.1).

3.3. Stable isotope composition of foraminiferal shells

The determination of carbon and oxygen isotope compositions ($\delta^{13}C$, $\delta^{18}O$) of 166 samples was carried out at the Institute of Geological Sciences of Polish Academy of Sciences in Warsaw. Each sample consisted of at least 12 clean specimens of the planktonic species *Orbulina universa.* Specimens were hand-picked, crushed, and ultrasonically cleaned with ethanol. Following the findings of Capotondi et al. (2002) for the Mediterranean region, specimens were collected from the 125 μm size fraction, providing the most reliable paleoclimatic and paleoceanographic reconstruction. Samples were subjected to reaction with 100% H_3PO_4 at 70 °C in an online, automated carbonate reaction device (Kiel IV), connected to the Finnigan Mat Delta Plus mass spectrometer. Isotope values have been referenced to the NBS19 standard. The reproducibility of the relevant determinations was <0.13‰ and < 0.08‰ (±1 s.d.) for $\delta^{18}O$ and $\delta^{13}C$ values, respectively.

3.4. Calcareous nannofossil analysis

One hundred seventy-four samples (~0.2 g of dry bulk sediment each) were selected for calcareous nannofossil (CN) analysis. A combined dilution/filtering technique was followed as described by e.g., Andruleit (1996), Baumann and Vollmar (2022). Samples were treated ultrasonically for a maximum of 60 s and then wet-split into 10 equal fractions using a rotary sample divider and buffered distilled water (pH > 8). Aliquots were further split into 10 equal fractions. A split fraction of each sample was filtered onto a Millipore cellulose nitrate filter (47 mm diameter, 0.45 μm pore size) using a vacuum pump. Quantitative analysis of CN was performed using a polarized Leica DMLSP (LM) at 1250× by counting 300 calcareous nannofossil specimens present within at least 3 fields of view (FOV). In addition, 7–15 extra FOVs were analysed for the minor species, ending to a total of at least 500 counted calcareous nannofossils per sample.

The absolute abundance of calcareous nannofossils (N) was calculated as:

$N=F \times C \times S/A \times W$, where N = number of calcareous nannofossil g^{-1} sediment, F = filtration area (mm^2), C = number of counted calcareous nannofossil specimens, S = split factor, A = counted area (mm^2) and W = sediment weight (g).

The CN absolute abundance was used to determine the calcareous nannofossil accumulation rate (CN AR; number of calcareous nannofossils cm^{-2} kyr^{-1}) based on the formula:

$CN\ AR = Dc \times DBD \times SR$, where Dc is calcareous nannofossils density (number of specimens of calcareous nannofossils per gram of sediment), DBD (g cm^{-3}) is the dry bulk density and SR is the sedimentation rate (for SR estimations see chapter 5.1 and Tables 3, 4). Following the approach of Bornemann et al. (2003), the wet bulk density (WBD; g cm^{-3}) and porosity (Φ; ranging from 44.26 to 46.35) from the DSDP Site 378 and 378A (Hsü et al., 1978) were used to derive the DBD values from the following equation $DBD = WBD - 1029 \times \Phi$, where Φ is the sediment porosity provided by Hsü et al. (1978) and 1.029 (g cm^{-3}) is the seawater density near the seabed of the deep Cretan Basin (Georgopoulos et al., 1989; Velaoras et al., 2014). The use of the previous equation assumes that the sediment is saturated with pore water. This is very likely to occur in the Cretan Basin, due to the high overburden pressures as well as due to the absence of natural gas north of Crete Island. Quantification of CN ARs is considered as especially important since it allows for a direct comparison with current surface sediment accumulation rates, past export production and partial carbonate dissolution (see e.g., Principato et al., 2006; Stolz and Baumann, 2010; González-Lanchas et al., 2021).

The relative abundance was calculated as the percentage of each taxon in the CN assemblages. In addition, the ratio between the two major taxa *Florisphaera profunda* (F) and small *Reticulofenestra* spp. < 5 μm (sR; mostly *R. minuta* and *R. haqii*) has been used as stratification index (S-index; modified from Flores et al., 2000). S=F/(F + sR), with increased S values indicating gradual establishment of water column stratification conditions and the onset of a nutrient-rich environment in the deep photic zone (Triantaphyllou et al., 2009).

Fifty-six additional samples were prepared to enhance the CN biostratigraphic analysis, following the standard smear slide techniques. The similarity in relative abundance of taxa collected using different preparation methods, i.e. smear slides standard techniques and filters (Baumann et al., 1998; Incarbona et al., 2011), ensures the reliability of data coming from the two different techniques, proving the consistency of these signals. The taxonomic concepts of the considered taxa followed the electronic guide to the biodiversity and taxonomy of calcareous nannoplankton Nannotax 3; http://www.mikrotax.org/Nannotax3/ (Young et al., 2022) (ina.tmsoc.org/Nannotax3/index.html).

Biostratigraphic assignment was performed by counting index species in a predetermined number of taxonomically related forms per sample. This method was applied to 50 specimens of discoasterids and 50 specimens of helicoliths, while for the stratigraphically significant but very rare taxa (e.g., Ceratolithaceae family) a minimum of 100 FOV

(with approximately the same density) were analysed, following the determination of the biostratigraphic events described by Backman et al. (2012). Zone assignment for the Site 378 record followed the biostratigraphic scheme of Agnini et al. (2017), Backman et al. (2012), and Di Stefano and Sturiale (2010), correlated to Martini (1971) standard biozones. The numerical age of the CN biozone boundaries is after Agnini et al. (2017). Additionally, nannofossil bioevents of Di Stefano and Sturiale (2010) identified in the Mediterranean region are used for the better constraint of the biostratigraphic assignment. Stage ages used correspond to Gradstein and Ogg (2020).

3.5. Spectral and statistical analyses

Following the approaches of Mitchell et al. (2008), a spectral analysis (using the PAST software package) was applied to the collected lithostratigraphic data to test the cyclic nature of the alternations between the lithological components. Before the data were applied to the periodogram, the lithological log was converted to a numerical string, assigning the values of 100 and 155 to the marly and sapropelic layers (based on Hsü et al., 1978), respectively.

R-mode Hierarchical Cluster Analysis (HCA) was performed on nannofossil species or genera that exceeded a relative abundance of 5% in at least two sediment samples. Statistical analysis (using the centroid linkage method and the distance metric of 1-Pearson correlation coefficient) was used to determine the calcareous nannofossil species associations. The analysis was accomplished using the SPSS (version 10.1) statistical software.

The age model of the Site 378 sedimentary record was performed in the QAnalySeries software (Kotov and Paelike, 2018). Using the biostratigraphic points to control the generated age model, QAnalySeries produced the age model after the matching process of visually selected $\delta^{18}O$ tie points for the cores 3A and 11Z with the target $\delta^{18}O$ curve (stack LR04; Lisiecki and Raymo, 2005). A total of 35 and 48 $\delta^{18}O$ tie points were selected in the cores 3A and 11Z, respectively (Tables 3, 4).

4. Results

4.1. Geochemical analysis in sediments (TOC, $\delta^{15}N$, $\delta^{13}C_{org}$)

The TOC content of the bulk carbonate samples ranges from 0.32 to 4.53%. The highest TOC concentration is observed within the sapropelic layers; maxima at 294 mbsf in core 3A (peak of 4.34%; Fig. 3a) and at 309–308.5 mbsf (peak of 4.53% at 309 mbsf; Fig. 3b) in core 11Z. In the marly layers, TOC is remarkably lower; minima occur at 309.8 mbsf in core 11Z and at 297.2 mbsf in core 3A (Fig. 3).

The $\delta^{15}N$ varies between −0.27 and 10.18‰ (Fig. 3), with minimum values occurring in sapropels. In core 3A, the highest $\delta^{15}N$ values are recorded at 301.8 and 299.7 mbsf in the marly layers, while the lowest value is recorded at 298.4 mbsf in a sapropelic layer. From 309.8 to 308.4 mbsf in core 11Z, several minima are noted, characterizing the indicated sapropelic layers and falling between some of the highest values recorded in the marly intervals.

The $\delta^{13}C_{org}$ varies from −24.95 to −21.96‰. Although no clear shifts are observed in core 3A, lower $\delta^{13}C_{org}$ values appear in the upper part of the core (Fig. 3a). In core 11Z, a slight $\delta^{13}C_{org}$ increase is recorded between 309.2 and 307.8 mbsf within the sapropelic layers. In contrast, two minima (−24.55‰, −24.33‰) are observed up to 307.2 mbsf (Fig. 3b). Apart from the previous abrupt drop, the $\delta^{13}C_{org}$ distribution in core 11Z does not display any large fluctuations.

4.2. Planktonic foraminifera $\delta^{18}O$ and $\delta^{13}C$ record

The $\delta^{18}O$ of the planktonic foraminifer *Orbulina universa* ranges from −0.33 to 1.31‰ VPDB in both studied cores (Fig. 3). The most significant negative $\delta^{18}O$ shifts are observed at the sapropelic layers between 298.2 and 296.9 mbsf in core 3A and at 309.1 to 308.4 mbsf in core 11Z. In contrast, maxima in $\delta^{18}O$ are observed in the marly intervals between 296 and 295 mbsf in core 3A and 306.3 to 306 mbsf in core 11Z.

The $\delta^{13}C$ of planktonic foraminifera tests, varies between −0.08 and 2.43‰ VPDB (Fig. 3), with minimum values to be recorded at 298.1 mbsf in core 3A and at 309.61 mbsf in core 11Z. In contrast, Fig. 3 shows relatively higher values at 301.6 mbsf and 308.3 mbsf, respectively (Fig. 3).

4.3. Calcareous nannofossil and planktonic foraminifera assemblage composition

In total, 57 different species were counted (species list in Table 5), of which the representative CN taxa are plotted in Fig. 4. In both cores, species from the Noelaerhabdaceae family dominate (*Reticulofenestra* spp. < 5 μm; up to 74%), together with the deep-photic taxon *Florisphaera profunda* (up to 64%); maxima of the latter species are recorded within the sapropelic layers (see Supplementary data). *Reticulofenestra pseudoumbilicus* (> 7 μm) although presenting an increment after 309.24 mbsf in core 11Z, never reaches more than 2%. Other important species in the assemblage composition are *Umbilicosphaera* spp. (*U. jafari, U. rotula*) and *Calcidiscus leptoporus,* with abundances of 32% and 18%, respectively, mostly abundant in the marly layers of both sedimentary records. In contrast, *Helicosphaera* spp. (*H. carteri* and *H. hyalina;* up to 15%) depict maxima in the sapropelic layers. *Helicosphaera sellii* values are increased after 308.33 mbsf in core 11Z and 300.32 mbsf in core 3A, respectively, but never exceed 3.6%. Discoasters are mainly represented by *D. brouweri* group and *D. pentaradiatus* specimens, with increased values often recorded in the sapropelic layers. The increase (> 10%) in the relative abundance of *D. asymmetricus* in relation to its ancestor species *D. brouweri* is observed in the uppermost section of both cores (3A: 295.96 mbsf; 11Z: 306.2 mbsf; Fig. 5). Significantly less frequent species are *Rhabdosphaera* spp. and *Sphenolithus* spp. (mostly *S. abies*), while the presence of *Syracosphaera pulchra* and *Pontosphaera discopora* is sporadic. Among the very rare Ceratolithaceae family, *Ceratolithus acutus* is absent in core 3A, while the species last occurrence in core 11Z is recorded at 309.4 mbsf, followed by the presence of *C. cristatus* at 309.14 mbsf (Fig. 5b).

The investigated record is characterized by generally low S-index values, with positive shifts up to 0.7 demonstrated within the sapropelic intervals, while it does not exceed 0.4 in the marly intercalations (Fig. 4).

R-mode HCA enables to identify two main groups in the calcareous nannofossil assemblages (Fig. 4c). Group I consists of two Subgroups (Ia, and Ib) including five taxa in total. Subgroup Ia includes *F. profunda*, *Sphenolithus* spp. and *Discoaster* spp., while Subgroup Ib comprises *Reticulofenestra* spp. and *Calcidiscus* spp. Finally, Group II consists of *Helicosphaera* spp., *R. clavigera* and *Umbilicosphaera* spp.

Globorotalia margaritae reaches 4% of the planktonic foraminifera assemblage for the first time at 309.6 mbsf in core 11Z, while the species becomes lower than 4% at 305.9 mbsf and at 295.4 mbsf in cores 11Z and 3A, respectively (Fig. 5). Values of species *Globorotalia puncticulata,* higher than 0.5%, are firstly detected at 308.1 mbsf in core 11Z and 299.6 mbsf in core 3A (Fig. 5).

5. Discussion

5.1. Biostratigraphy and Site 378 combined age model

The biostratigraphic analysis is based on the detection of certain CN biohorizons (Di Stefano and Sturiale, 2010; Agnini et al., 2017, Fig. 5). In particular, the occurrence of *C. acutus* recorded only in the basal part of core 11Z enables correlation with the CN biozone NN12 (Martini, 1971), which corresponds to biozone CNPL1 (Backman et al., 2012; Agnini et al., 2017). Accordingly, the Top (T) of *C. acutus* occurs at 309.4 mbsf in the core 11Z; this bioevent, absent in core 3A, is followed by the

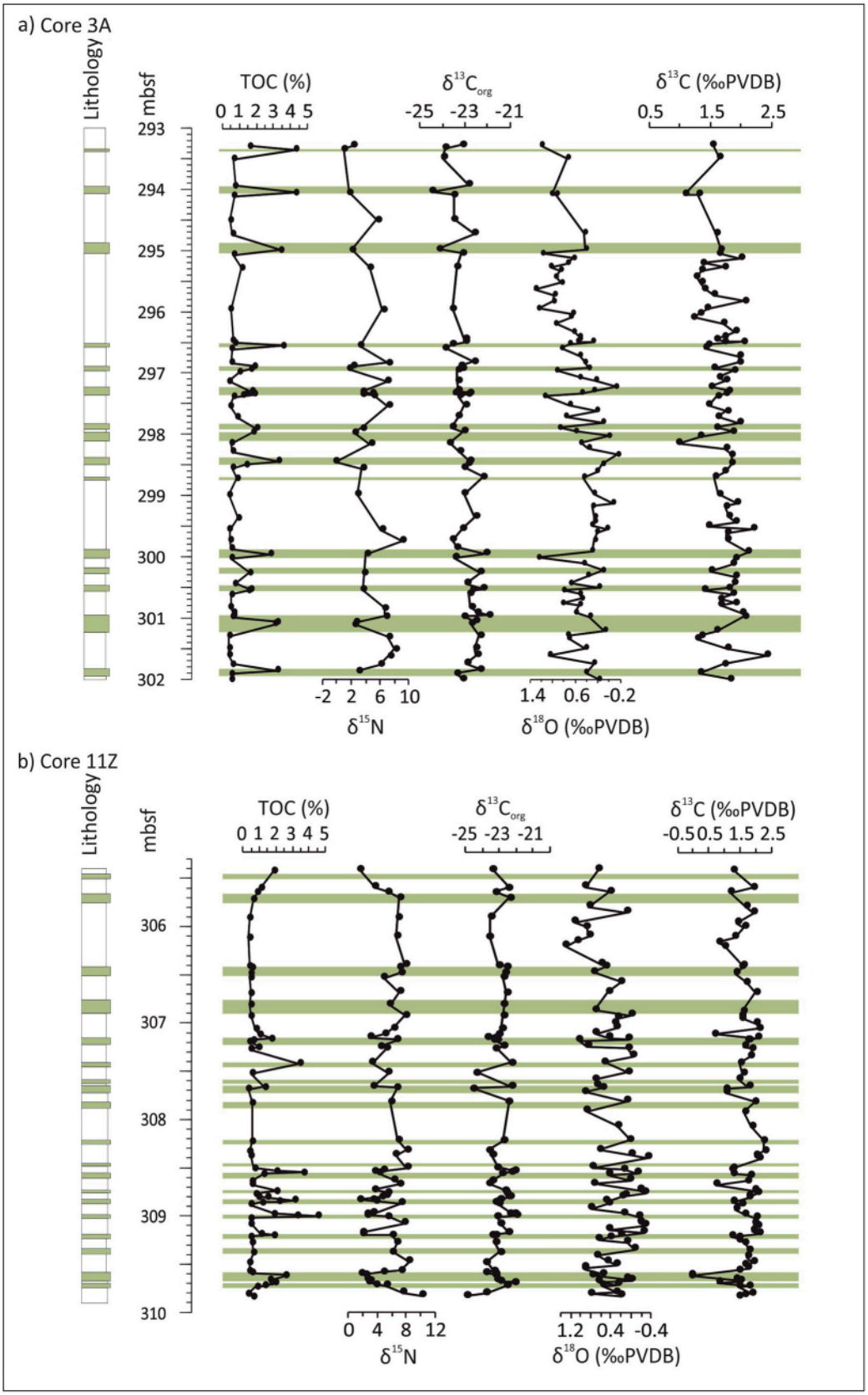

Fig. 3. Geochemical results in (a) Core 3A, (b) Core 11Z. Position of sapropels is according to Hsü et al. (1978).

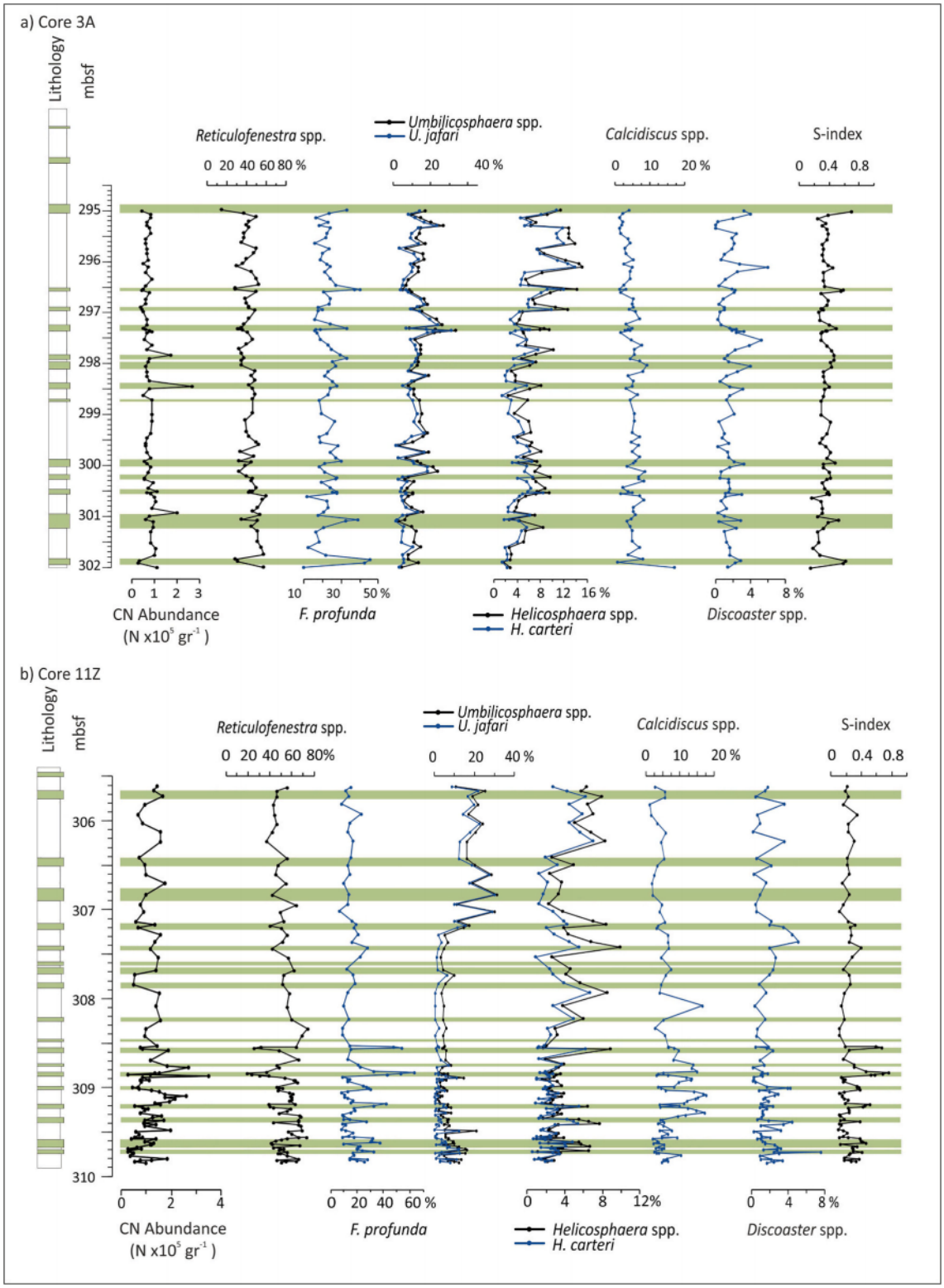

Fig. 4. Calcareous nannofossil absolute abundance, dominant species relative abundance and S-index in (a) Core 3A and (b) Core 11Z. Position of sapropels is according to Hsü et al. (1978). (c) R-mode Hierarchical Cluster Analysis (HCA; centroid linkage method, distance metric is 1- Pearson correlation coefficient) of the major calcareous nannofossil species.

presence of *C. cristatus* (Fig. 5b), marking the boundary of CNPL1/CNPL2 biozones, dated at 5.04 Ma. Even though *C. acutus* is recorded in both western (e.g., Site 975B in Di Stefano and Sturiale, 2010) and eastern Mediterranean sites (e.g., Site 969B in Di Stefano and Sturiale, 2010; Zakynthos Island in Karakitsios et al., 2017), the reliability of this bioevent is still on sharp disagreement (e.g., Popescu et al., 2007, 2008; Roveri et al., 2008; Andreetto et al., 2021). Several studies suggested its low applicability in the Mediterranean, due to *C. acutus* rare presence in

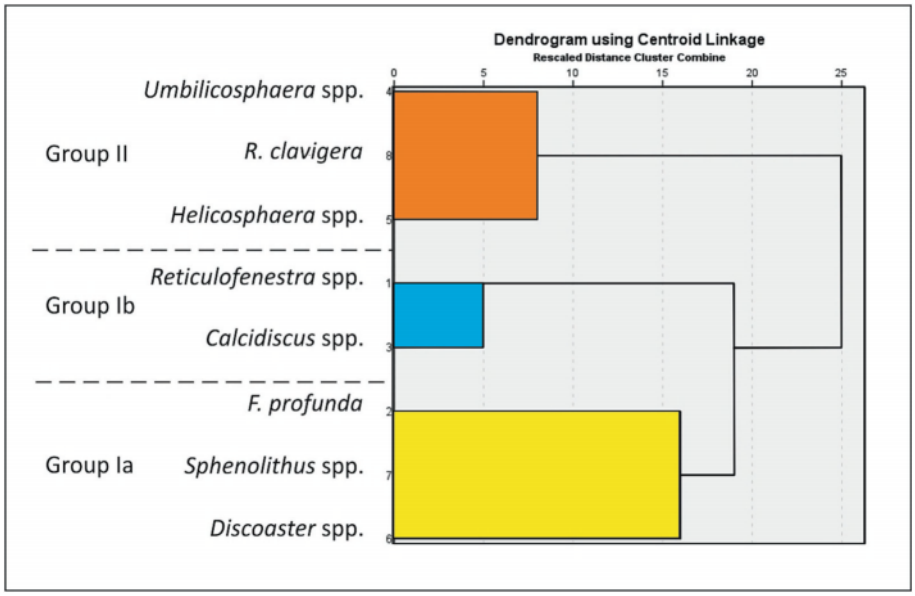

Fig. 4. (*continued*).

the area (e.g. Roveri et al., 2008; Di Stefano and Sturiale, 2010). In contrast, even in very low frequency, Popescu et al. (2008) and Karakitsios et al. (2017) proved the species identification with a "longer than routine" investigation; i.e. similarly to the one applied to the studied core 11Z. Moving upwards, the absence of *Reticulofenestra zancleana* and the concomitant *R. pseudoumbilicus* Paracme "P" End (P"P"E) observed at 5.004 Ma in core 11Z, marks biozone MNN12b of Di Stefano and Sturiale (2010), while biozone MNN12c up to the FCO of *H. sellii* (4.62 Ma; Di Stefano and Sturiale, 2010) is detected in both cores. Similar to previous studies in the eastern Mediterranean (e.g., Site 969B, Di Stefano and Sturiale, 2010), both cores of the present study recorded the FCO of *H. sellii* with low abundance (<3.6%). Towards the top, the Base common (Bc) of *D. asymmetricus*, verifies the CNPL2/CNPL3 biozone boundary (4.04 Ma; Backman et al., 2012; Agnini et al., 2017) (Table 2; Fig. 5).

Three planktonic foraminiferal events associated with four planktonic foraminiferal biohorizons, can be used to confirm the age model (Table 2; Fig. 5). *Globorotalia margaritae* FCO occurrs at 5.08 Ma in core 11Z, corresponding to the top of biozone MPL1, while this bioevent is absent from core 3A. Upwards, *Globorotalia puncticulata* is firstly detected at 308.1 mbsf in core 11Z and at 299.6 mbsf in core 3A, defining *Globorotalia puncticulata* FO that marks the top of biozone MPL3 at 4.52 Ma. Finally, *G. margaritae* LCO (3.98 Ma), observed at 305.9 mbsf in core 11z and at 295.4 mbsf in core 3A, indicates the boundary of the MPL3–MPL4 biozones.

Thus, the documented biostratigraphic intervals, when considering both investigated records, correspond to the ~5.08–3.98 Ma time interval, placing the studied sequence in the Zanclean, Early Pliocene (Table 2).

To refine the provided stratigraphy of the studied sequence, the $\delta^{18}O$ record of each core has been graphically correlated with the LR04 astronomically tuned global benthic foraminifera $\delta^{18}O$ stack (Fig. 6; abbreviations after Tables 2, 3, 4). The use of LR04 stack as an initial alignment target supposes the synchronous trends of benthic and planktonic $\delta^{18}O$. Recently, Bowman et al. (2023) proved the good agreement in age model for the portion of planktonic stack constrained by radiocarbon data, to the equivalent of the LR04 global benthic $\delta^{18}O$ stack, suggesting that age estimates for planktonic and benthic $\delta^{18}O$ are similar on orbital time scales. Indeed, the produced age-to-$\delta^{18}O$ profiles in both cores of Site 378 show a significant positive correlation (~0.7) with the target isotopic stack (red line; Fig. 6). Even taking into account that the benthic stack resolution is higher, our planktonic isotope record exhibits 57 out of the total 62 isotopic stages in the Early Pliocene targeted interval, further supporting the sufficient comparison. The precipitation patterns on the surrounding areas, including the African monsoonal activity and riverine inputs, might have a strong influence on the Pliocene hydroclimate of the Aegean. However, the global to local scale application of the LR04 stack in several studies (e.g., Di Stefano et al., 2015; Athanasiou et al., 2017; Grant et al., 2022) has been so far proven to efficiently detect the eastern Mediterranean paleoenvironmental conditions.

Based on the defined biostratigraphic tie points and the $\delta^{18}O$ record tuning outcomes (Tables 2, 3, 4), a continuous linear regression-derived age model has been generated for each studied core. Sedimentation rates fluctuate throughout the analysed cores (Fig. 6), with average rates of 0.4 cm/kyr in core 11Z and 0.9 cm/kyr in core 3A. The difference in the previous values should be due to the combined effect of the sub-bottom geometry of sediment layers in the sampling site (the northern flank of a seabed depression; see seismic profile in Hsü et al., 1978) and the accuracy in the position of the two "replicate" Holes 378 and 378A on the seafloor.

In order to confirm the main periodicities and the phase relationships relative to the astronomical forcing, the datasets obtained from both cores were processed following the spectral analysis approach of Mitchell et al. (2008) (Fig. 6). The numerical string of the lithology in both cores exhibits a significant periodic signal corresponding to the 23-kyr cycle of orbital precession, in agreement to the cyclicity described in the Early Pliocene Capo Rosello Composite Section (CRCS; Langereis and Hilgen, 1991; Fischer et al., 2009). A secondary periodic signal of 48 kyr reveals the additional impact of obliquity in the cyclicity of core 3A.

The derived age models enabled all geochemical and micropaleontological data from both cores studied, to be sorted by age as a combined single record. The first-order bed-to-bed age control through the comparison with the CRCS sapropel sequence (Hilgen, 1991; Lourens et al., 1996; Wang et al., 2010), resulted to the tuning of Site 378 sapropelic cycles to the La2004 solution (Laskar et al., 2004), implying the astronomical calibration of the combined sapropel dataset with the i-cycles 490–374 (5.195–3.875 Ma) (Fig. 7). Few additional "ghost" sapropelic layers have been detected (see gray bands in Fig. 7), based on their TOC content and the estimated stratification S-index, coupled with the simultaneous negative shifts in the $\delta^{15}N$, $\delta^{18}O$ and $\delta^{13}C$ profiles. Clearly, the sapropelic-marly couplets pattern observed at the Cretan site is

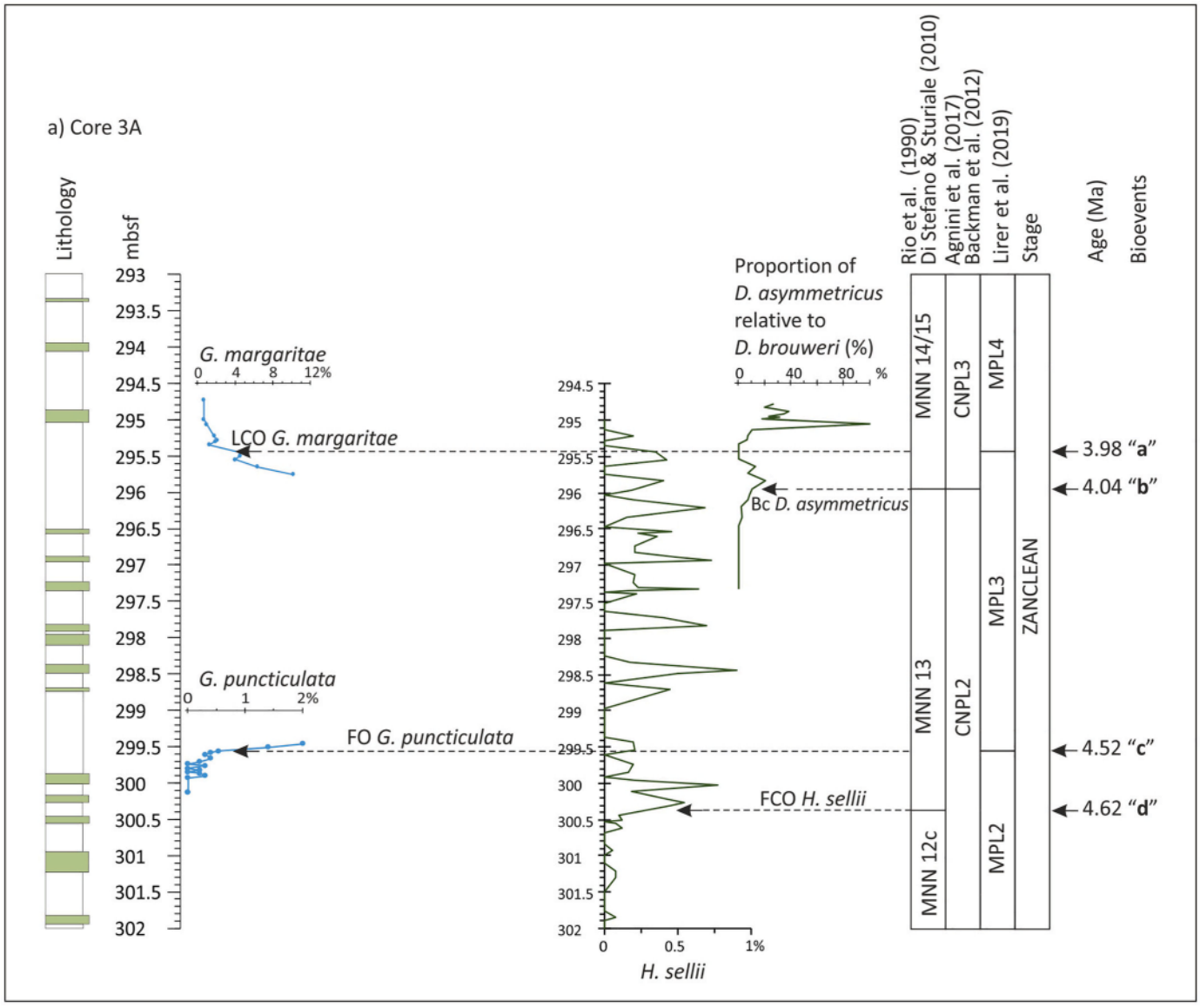

Fig. 5. (a) Core 3A, (b) Core 11Z: Calcareous nannofossil biostratigraphic assignment, following Martini (1971) and Backman et al. (2012) nannofossil zonal schemes; ages are after Agnini et al. (2017). Abbreviations as follows: Bc-Base common, T-Top. Foraminiferal biostratigraphic points following Lirer et al. (2019). Abbreviations as follows: FCO-First Common Occurrence, FO-First Occurrence, LCO-Last Common Occurrence, Paracme "P" End ($P_{..p..}E$). Age (Ma) after Gradstein and Ogg (2020). Position of sapropels is according to Hsü et al. (1978).

much simpler than the cyclic Early Pliocene quadruplets of CRCS record, rather resembling to the Calabrian Trubi marl doublets (Hilgen, 1987) and the Early Pliocene ODP Site 978 couplets in the Alboran Sea (Marsaglia et al., 2004).These precessional-controlled couplets in the Mediterranean are attributed to the regional atmosphere-ocean feedback system (Thunell et al., 1991; Lourens et al., 1996), representing the maximum seasonality during summer and winter perihelion phases (Fischer et al., 2009).

5.2. Early Pliocene paleoceanographic reconstruction

Precessional climate changes have been identified as the main factor of Mediterranean surface water freshening and sapropel formation (Rossignol-Strick, 1985). The concept of sapropels was initially attributed to increased TOC preserved under anoxic conditions (Olausson, 1961; Kidd et al., 1978); however, high TOC should be also explained by higher primary productivity levels (Pedersen and Calvert, 1990). To unravel the environmental changes in the water column of the Cretan Basin, the CN ARs have been calculated (average of 9.24×10^4 CN cm^{-2} kyr^{-1}; Fig. 8a) as an effective primary productivity proxy (e.g., Principato et al., 2006; Stolz and Baumann, 2010; Athanasiou et al., 2017; Cavaleiro et al., 2018; Skampa et al., 2019).

In between ~5.2–4.6 Ma, the CN assemblage is dominated by *Reticulofenestra* spp. (average AR of 4.3×10^4 CN cm^{-2} kyr^{-1}; Fig. 8a), a typical component of meso- to eutrophic surface waters (e.g., Flores et al., 2005). In the same time, the accumulation of *F. profunda* is moderate; few sporadic peaks within sapropelic layers are recorded up to ~4.4 Ma, with max. value at i-cycle 470 (Fig. 8a). *Florisphaera profunda* is featuring the sapropel CN assemblages in times of increased North African humidity during the precession minima (Castradori, 1998). The species is considered to be restricted to the light-limited, lower photic zone of the tropical and subtropical environments including Mediterranean (e.g., Molfino and McIntyre, 1990), pointing to the enhanced stratification of the water column and productivity in the

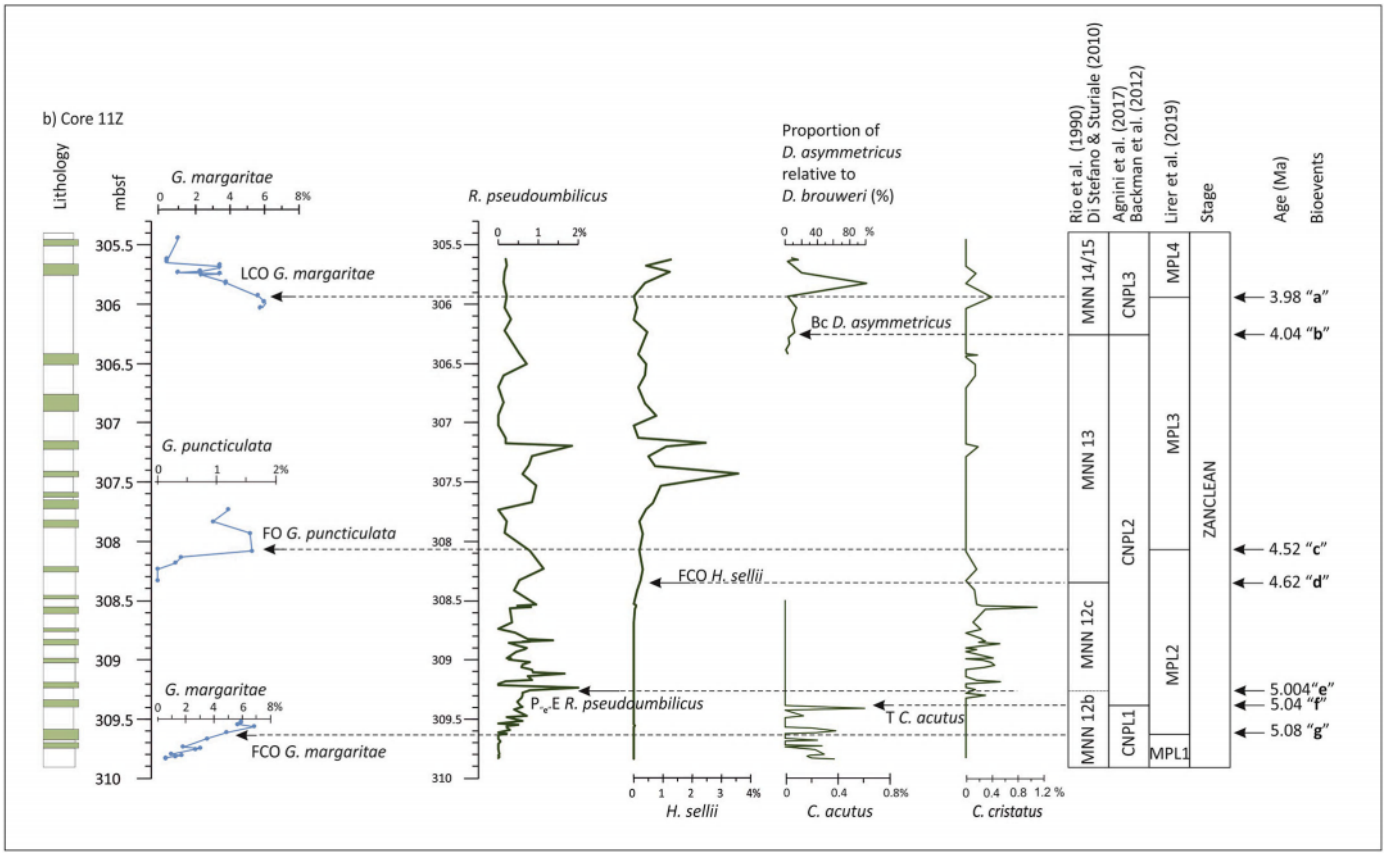

Fig. 5. (*continued*).

Table 2
Calcareous nannofossil and planktonic foraminifera biohorizons used in the present study. Meters Below Sea Floor (mbsf) in each studied Core.

Age (Ma)	Reference	Biohorizon	mbsf Core 3A	mbsf Core 11Z
3.98	Lirer et al. (2019)	**"a"** LCO *Globorotalia margaritae*	295.44	305.93
4.04	Agnini et al. (2017)	**"b"** Bc *Discoaster asymmetricus*	295.96	306.23
4.52	Lirer et al. (2019)	**"c"** FO *Globorotalia puncticulata*	299.55	308.08
4.62	Di Stefano and Sturiale (2010)	**"d"** FCO *H. selli*	300.38	308.35
5.004	Di Stefano and Sturiale (2010)	**"e"** P-e-E *R. pseudoumbilicus*	–	309.25
5.04	Agnini et al. (2017)	**"f"** T *Ceratolithus acutus*	–	309.38
5.08	Lirer et al. (2019)	**"g"** FCO *Globorotalia margaritae*	–	309.61

deep photic zone. The i-cycle 470 is coupled with the prominent negative shift of $\delta^{18}O$ in the warm marine event Si5, and simultaneous lighter $\delta^{15}N$ values (Fig. 7), further supporting the development of stagnation and low oxygen conditions (e.g., Arnaboldi and Meyers, 2006).

Used as opportunistic warm and mesotrophic deep-water indicators, occasionally adapted to high salinity fluctuations (e.g., Wade and Bown, 2006), *Sphenolithus* spp. additionally testify the DCM signal. *Sphenolithus* spp., although with much lower ARs, are also peaking mostly before ~4.6–4.4 Ma, within sapropel cycles 470, 468, 450, 424. The even rarer *Discoaster* spp., with several abundance peaks up to ~4.6–4.4 Ma, coupled with negative $\delta^{15}N$ shifts, i.e., in the high TOC sapropel cycle 424 (Figs. 7, 8a), are also indicative of favourable conditions for productivity in the deep photic zone, as they are considered to flourish in warm, and stratified waters during Miocene and Pliocene (Vázquez et al., 2000; Athanasiou et al., 2015, 2021). However, despite the notable presence of the deep dwellers, the elevated ARs of *Reticulofenestra* spp. in the sapropel cycles 490–442 (Fig. 8a) suggest nutrient dispersal throughout the water column, resulting in concurrent rise of surface primary productivity (Hernández-Almeida et al., 2019), equally to the "placolith-controlled" conditions also documented in the Holocene sapropel S1 (Incarbona et al., 2011). The $\delta^{13}C_{org}$ displays slightly depleted values in relation to pure algal productivity (−18 to −22‰; Arnaboldi and Meyers, 2006); a plausible explanation may include the contribution of terrestrial organic matter, mainly via atmospheric and riverine inputs and/or drawdown of dissolved $^{12}CO_2$ (Gogou et al., 2007; Katsouras et al., 2010), similar to previous studies (Nijenhuis and de Lange, 2000; Lamb et al., 2006). Hence, the water column nutrient enrichment could be mostly due to relatively increased riverine fluxes before ~4.6 Ma, as also described by Grant et al. (2022). Still, the distinctive positive $\delta^{13}C_{org}$ shifts at ~4.9 to 5 Ma, might signify the beginning of the following interval with decreased precipitation in the eastern Mediterranean (e.g., Di Stefano et al., 2015), pinpointing to reduced riverine inputs.

Interestingly, the accumulation of *F. profunda* in the Cretan Basin record (average ARs of 2.4×10^4 CN cm^{-2} kyr^{-1}) is low in comparison to the much more enhanced accumulation rates in the Levantine (on land Cyprus) Pliocene sequences (appr. 2×10^7 CN cm^{-2} kyr^{-1}; Athanasiou et al., 2017), implying significant disparities in the water column structure of the different basins as also differences in the surface productivity (Hernández-Almeida et al., 2019). In the same line, the striking absence of *F. profunda* in the CRCS sequence of the central Mediterranean (Beltran et al., 2011; Plancq et al., 2015), further emphasizes the different processes in the efficiency of deep-water renewal between the western and eastern Mediterranean during sapropel deposition (e.g., Bouloubassi et al., 1999; Cacho et al., 2001; Rohling et al., 2015). The

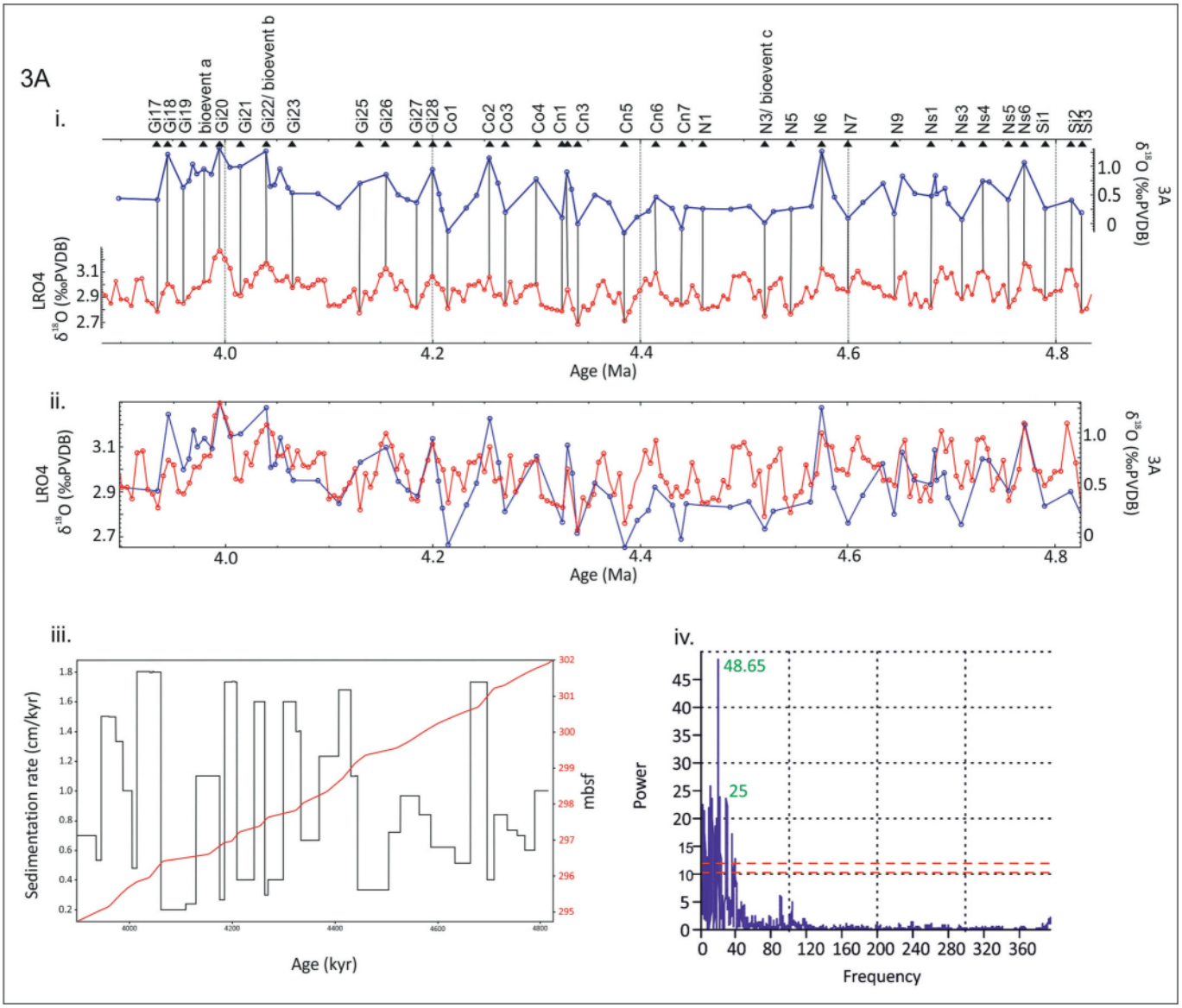

Fig. 6. (a) i. Tie points (black triangles: Isotopic Stages and Bioevents used to control the generated age model) applied for tuning Site 378 Core 3A with the target curve of global marine $\delta^{18}O$ LR04 stack (red line; Lisiecki and Raymo, 2005), ii. final correlation scheme, iii. Sedimentation rates in Core 3A, iv. power analysis of the lithological variations in Core 3A. (For interpretation of the references to colour in this figure legend, the reader is referred to the web version of this article.) (b) i. Tie points (black triangles: Isotopic Stages and Bioevents used to control the generated age model) applied for tuning Site 378 Core 11Z with the target curve of global marine $\delta^{18}O$ LR04 stack (red line; Lisiecki and Raymo, 2005), ii. final correlation scheme, iii. Sedimentation rates in Core 11Z, iv. power analysis of the lithological variations in Core 11Z. (For interpretation of the references to colour in this figure legend, the reader is referred to the web version of this article.)

remarkably high abundance of *F. profunda* close to the LIW source in the Levantine Basin, has been interpreted as a forceful DCM signal within the Pliocene and Quaternary/Holocene sapropels (Castradori, 1998; Principato et al., 2006; Athanasiou et al., 2017). This is explained by the LIW presence at shallower depth in the eastern Mediterranean, compared to the western part, which favoured the shoaling of the DCM through enhanced upward injection of nutrients (Grelaud et al., 2012). The faint expression of this mechanism in Site 378, clearly depicted in *F. profunda* moderate values, may suggest that LIW formation was not strong enough to properly reach the Cretan Basin in the beginning of the Pliocene, hence weakly affecting the Cretan water column during ~5.2–4.6 Ma (Fig. 9a). LIW presence testified in the central Mediterranean area only since middle Pliocene (Roveri, 2002), further confirms this speculation.

In the following ~4.6–3.9 Ma time interval, Group Ia, including recorded maxima of CN deep photic zone dwellers in the sapropelic layers, presents an overall decrease (cycles 440–374). Similarly, Group Ib, characterizing both low-TOC marls and sapropelic layers, is featured by an overall declining trend of the dominant *Reticulofenestra* spp. that implies nutrient reduction in the upper part of the water column. A comparable reducing AR pattern is shown in *Calcidiscus* spp., a taxon related with nutrient-rich settings (e.g., Baumann et al., 2016). Furthermore, the AR decrease of small to medium-size reticulofenestrids, reflecting stable water conditions, normal salinities and increased availability of terrigenous nutrients (e.g., Di Stefano et al., 2015), suggests that this interval was characterized by riverine inflow slowdown. The shift to higher $\delta^{15}N$ values (Fig. 7), further testifies well mixed water column conditions probably related to the runoff decrease (Arnaboldi and Meyers, 2006; Higgins et al., 2010), directly related to the fall in precipitation (Van Dam, 2006; Grant et al., 2022).

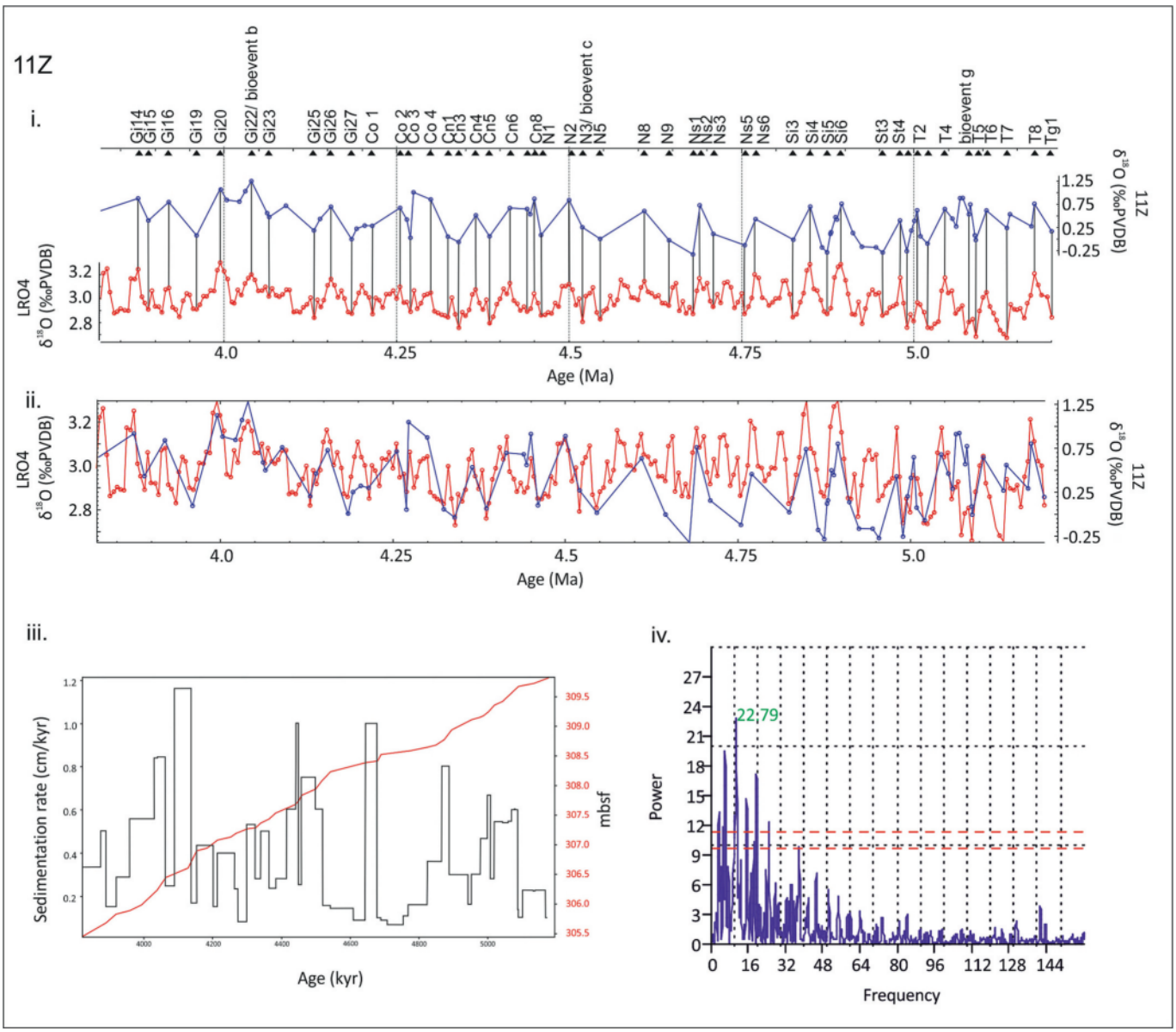

Fig. 6. (*continued*).

Interestingly, these conditions were not affecting only the South Aegean Cretan Basin but also the Adriatic as well (Di Stefano et al., 2015).

In contrast, Group II, featuring primarily the sapropelic layers, depicts an overall increment that clearly expands in abundance after cycle 442 (4.6 Ma; Fig. 8b). The group mainly consists of *Helicosphaera* spp., associated with enhanced freshwater inputs during sapropel deposition in the eastern Mediterranean (e.g., Triantaphyllou et al., 2009, 2016; Athanasiou et al., 2017, 2021), and the upper-photic zone flourishing species *Umbilicosphaera* spp. and *Rhabdosphaera* spp., which generally characterize warm and oligotrophic surface waters (e.g., Palumbo et al., 2013). Previous record of *U. jafari* in the eastern Mediterranean (e.g., Wade and Bown, 2006; Athanasiou et al., 2015) stated the species ability to thrive in high salinity environments. Nevertheless, when studying the coccolithophore export production at the southwestern margin of Crete, Malinverno et al. (2009) have recorded the dominance of *Umbilicosphaera* spp. and *H. carteri* linked to increased nutrient availability during maxima in precipitation and water column mixing. Thus, the dominance of *H. carteri* in the sapropel cycles 440–374 of the Cretan Basin record (Fig. 8a), besides freshening, also presumes mesotrophic conditions in the mid photic zone close to the chlorophyll maximum (Corselli et al., 2002). In agreement with the prominent fluctuations of *Rhabdosphaera* spp. after 4.6 Ma, which demonstrate the predominance of oligotrophic surface waters in a fairly well stratified water column, the concomitant increased occurrence of *Umbilicosphaera* spp., especially within the marly layers, is also considered to be associated with the increase in productivity and salinity of the mid photic zone. Similar increase in warm-water taxa combined with reduction in medium-size reticulofenestrids, was previously recorded at 4.92 Ma at ODP Site 696B (Mediterranean Ridge), depicting the transition from normal open-ocean cool conditions to more restricted marine environments characterized by higher salinities and water temperatures (Di Stefano et al., 2015).

Evidently, the mid photic zone productivity after ~4.6 Ma, implied by the increase of Group II in the sapropelic layers and the salinity index *U. jafari* in the alternating marly intervals, (Figs. 4, 8), confirms the presence of warm, saline and nutrient rich water masses in intermediate water depths, thus a stronger LIW impact in the South Aegean Cretan Basin, in between ~4.6–3.9 Ma (Fig. 9b). Inevitably, the formation of the warm, saline, and nutrient enriched LIW masses (Parras-Berrocal et al., 2023) and the corresponding shoaling of the pycnocline/

Table 3
Depth occurrence of tuning $\delta^{18}O$ tie points, bioevents used for the age model and sedimentation rates in Core 11Z.

Core 11Z Depth (mbsf)	Age (Ma)	Isotopic Stages and Bioevents used in the 11Z tuning with LR04 target $\delta^{18}O$ curve	Additional bioevents used for the age model	Sedimentation Rate (cm/kyr)
305.62	3.875	Gi14		0.33
305.67	3.89	Gi15		0.50
305.82	3.92	Gi16		0.15
305.88	3.96	Gi19		0.25
			bioevent a (LCO *G. margaritae*)	
305.93	3.98			0.33
305.98	3.995	Gi20		0.56
		Gi22/ bioevent b (Bc *D. asymmetricus*)		
306.23	4.04			0.84
306.44	4.065	Gi23		0.25
306.6	4.13	Gi25		1.16
306.89	4.155	Gi26		0.17
306.94	4.185	Gi27		0.43
307.07	4.215	Co1		0.15
307.13	4.255	Co2		0.40
307.19	4.27	Co3		0.23
307.26	4.3	Co4		0.08
307.28	4.325	CN1		0.53
307.36	4.34	CN3		0.28
307.43	4.365	CN4		0.50
307.53	4.385	CN5		0.23
307.6	4.415	CN6		0.28
307.67	4.44	CN7		0.60
307.73	4.45	CN8		1.00
307.83	4.46	N1		0.25
307.93	4.5	N2		0.75
		N3/ bioevent c (FO *G. puncticulata*)		
308.08	4.52			0.60
308.23	4.545	N5		0.15
308.33	4.61	N8		0.2
			bioevent d (FCO *H. selli)*	
308.35	4.62			0.12
308.38	4.645	N9		0.09
308.41	4.68	NS1		1.00
308.51	4.69	NS2		0.10
308.53	4.71	NS3		0.09
308.57	4.755	NS5		0.07
308.58	4.77	NS6		0.11
308.64	4.825	Si3		0.16
308.68	4.85	Si4		0.36
308.77	4.875	Si5		0.80
308.93	4.895	Si6		0.30
309.11	4.955	ST3		0.16
309.15	4.98	ST4		0.30
309.18	4.99	T1		0.43
			bioevent e (P. pseudoumbilicus)	
309.24	5.004			1
309.25	5.005	T2		0.67
309.35	5.02	T3		0.15
			bioevent f (T *C. acutus*)	
309.38	5.04			0.80
309.42	5.045	T4		0.54
		bioevent g (FCO *G. margaritae*)		
309.61	5.08			0.60
309.67	5.09	T5		0.13
309.69	5.105	T6		0.10
309.72	5.135	T7		0.22
309.81	5.175	T8		0.10
309.83	5.195	TG1		

Table 4
Depth occurrence of tuning $\delta^{18}O$ tie points, bioevents used for the age model and sedimentation rates in Core 3A.

Core 3A Depth (mbsf)	Age (Ma)	Isotopic Stages and Bioevents used in the 3A tuning with LR04 target $\delta^{18}O$ curve	Additional bioevents used for the age model	Sedimentation Rate (cm/kyr)
294.99	3.935	Gi17		0.7
295.06	3.945	Gi18		0.5
295.14	3.96	Gi19		1.5
295.44	3.98	bioevent a (LCO *G. margaritae*)		1.3
295.64	3.995	Gi20		1.0
295.84	4.015	Gi21		0.5
295.96	4.04	Gi22/ bioevent b (Bc *D. asymmetricus*)		1.8
296.41	4.065	Gi23		0.2
296.54	4.13	Gi25		0.2
296.6	4.155	Gi26		1.1
296.93	4.185	Gi27		0.3
296.97	4.2	Gi28		1.7
297.23	4.215	Co1		0.4
297.39	4.255	Co2		1.6
297.63	4.27	Co3		0.3
297.72	4.3	CO4		0.4
297.82	4.325	CN1		1.6
297.9	4.33	CN2		1.4
298.04	4.34	CN3		0.7
298.34	4.385	CN5		1.2
298.71	4.415	CN6		1.7
299.13	4.44	CN7		1.1
299.35	4.46	N1		0.3
299.55	4.52	N3/ bioevent c (FO *G. puncticulata*)		0.7
299.73	4.545	N5		1.0
300.02	4.575	N6		0.8
300.23	4.6	N7		0.6
300.38	4.62		bioevent d (FCO *H. selli*)	0.52
300.51	4.645	N9		0.5
300.69	4.68	NS1		1.7
301.21	4.71	NS3		0.4
301.29	4.73	NS4		0.8
301.5	4.755	NS5		0.7
301.61	4.77	NS6		0.7
301.75	4.79	Si1		0.6
301.9	4.815	Si2		1.0
302	4.825	Si3		

nutricline at shallow water depths, as also witnessed by the slight shift to more negative $\delta^{13}C_{org}$ (Katsouras et al., 2010), have triggered the nutrient availability and productivity enhancement in the mid-lower photic zone. LIW intensification is assumed to eject warmer and saltier water masses to the whole eastern Mediterranean. As a potential outcome, alterations of the deep water formation areas between Adriatic and Aegean Seas already predicted from model projections (Parras-Berrocal et al., 2023), similar to the EMT event mechanism (Velaoras et al., 2017), or other possible EMT-like phenomena (Gačić et al., 2012) should have taken place, enhancing the area's thermohaline circulation. Indeed, the continuous presence of marly-sapropel alterations suggests that precession oscillations remain the controlling mechanism of seasonally depicted marl-sapropel couplet deposition in the basin (Figs. 7, 8). However, notably cooler conditions in the intercalated low-OC marly layers of cycles 440–374 are documented by heavier $\delta^{18}O$ and the contemporaneous increment of $\delta^{15}N$ values that point to the prevalence of well mixed oxygenated waters (Higgins et al., 2010), representing the maximum seasonality during winter perihelion phases (e.g., Fischer et al., 2009), potentially enhanced by EMT-like events. In accordance, the concurrent isotopic negative shift interpreted as the expression of the cold MIS N6 and the following general cooling trend towards the cold MIS Gi20 at ~4.0 Ma (Fig. 7), mark the expression of the pronounced Northern Hemisphere ice volume expansion in the Cretan Basin, inevitably coupled with the strengthening of thermohaline circulation in the area.

Our data reveal that precession based climatic changes drove the Mediterranean Early Pliocene intermediate circulation on a seasonally controlled cold/faster (and well-ventilated) - warm/slower (and poorly ventilated) pattern, consistent with the present-day response of the LIW to seasonal oscillations (Toucanne et al., 2012). LIW formation

Table 5
Calcareous nannofossil species identified in this study.

Amaurolithus brevigracilis de Kaenel & Bergen, in de Kaenel et al. 2017
Amaurolithus delicatus Gartner and Bukry, 1975
Amaurolithus tricorniculatus (Gartner, 1967) Gartner and Bukry, 1975
Braarudosphaera bigelowii (Gran & Braarud, 1935) Deflandre, 1947
Calcidiscus leptoporus (Murray & Blackman, 1898) Loeblich & Tappan, 1978
Calcidiscus macintyrei (Bukry & Bramlette, 1969) Loeblich & Tappan, 1978
Calciosolenia Gran 1912 emend. Young et al. 2003
Ceratolithus acutus Gartner and Bukry, 1974
Ceratolithus cristatus Kamptner, 1950
Coccolithus pelagicus (Wallich, 1877) Schiller, 1930
Discoaster Tan, 1927
Discoaster brouweri var. *triradiatus* Tan, 1927b sensu Backman and Shackleton (1983)
Discoaster brouweri-like preservational morphotypes
Discoaster asymmetricus (Gartner, 1969)
Discoaster brouweri (Tan, 1927), emend. Bramlette and Riedel, (1954)
Discoaster decorus (Bukry 1971) Bukry 1973
Discoaster pansulus Browning & Bergen, in Browning et al. 2017
Discoaster pansus (Bukry & Percival, 1971) Bukry, 1973
Discoaster pentaradiatus (Tan, 1927), emend. Bramlette& Riedel (1954)
Discoaster surculus (Martini and Bramlette, 1963),
Discoaster tamalis (Kamptner, 1967)
Discoaster variabilis Martini & Bramlette, 1963
Discosphaera tubifera (Murray & Blackman 1898) Ostenfeld, 1900
Florisphaera profunda (Okada & Honjo, 1973)
Gephyrocapsa (small) Kamptner, 1943
Hayaster perplexus (Bramlette & Riedel 1954) Bukry, 1973
Helicosphaera carteri (Wallich, 1877) Kamptner, 1954
Helicosphaera hyalina Gaarder, 1970
Helicosphaera intermedia Martini, 1965
Helicosphaera princei da Gama & Varol 2013
Helicosphaera sellii (Bukry and Bramlette, 1969) Jafar and Martini, 1975
Helicosphaera wallichii (Lohman, 1902) Okada and McIntyre, 1977
Oolithotus fragilis (Lohmann 1912) Martini & Müller, 1972
Pontosphaera discopora Schiller, 1925, Varol, 1982
Pontosphaera japonica (Takayama 1967) Nishida, 1971
Pontosphaera multipora (Kamptner, 1948) Roth, 1970
Reticulofenestra haqii Backman, 1978
Reticulofenestra minuta Roth, 1970
Reticulofenestra minutula (Gartner, 1967) Haq & Berggren, 1978
Reticulofenestra pseudoumbilicus (Gartner, 1967), Gartner, 1969 > 7 μm
Rhabdosphaera clavigera Murray & Blackman, 1898
Scyphosphaera apsteinii forma dilatata Gaarder, 1970
Scyphosphaera apsteinii Lohmann, 1902
Scyphosphaera globulata Bukry and Percival, 1971
Scyphosphaera intermedia Deflandre, 1942
Scyphosphaera lagena Kamptner, 1955
Scyphosphaera pulcherrima Deflandre, 1942
Scyphosphaera ventriosa Martini, 1968
Sphenolithus abies Deflandre, in Deflandre & Fert, 1954
Sphenolithus Deflandre, 1952
Sphenolithus moriformis (Brönniman & Stradner, 1960) Bramlette & Wilcoxon, 1967
Sphenolithus neoabies Bukry & Bramlette 1969
Syracosphaera mediterranea Lohmann 1902
Syracosphaera pulchra Lohmann, 1902
Umbilicosphaera jafari Müller, 1974
Umbilicosphaera Lohman, 1902
Umbilicosphaera rotula (Kamptner, 1956), Varol, 1982

increment and high flow velocity has been observed under cold waters, i.e., winter seasonal cycles, glacial MIS and Heinrich Stadial events (Lascaratos et al., 1993; Roveri, 2002; Toucanne et al., 2012; Colin et al., 2021). Therefore, the prevalence of colder conditions is expected to enhance the eastern Mediterranean intermediate and deep convection regime (Toucanne et al., 2012), resulting in the intensified presence of the intermediate depth LIW mass, similarly to the circulation mechanisms of the last climatic cycle (e.g., Lascaratos et al., 1993; Toucanne et al., 2012; Colin et al., 2021); however LIW outflow might have weakened towards the western Mediterranean basin, much alike to the glacial circulation (Colin et al., 2021). Previous studies in eastern Mediterranean underlined the efficiency of EMT and associated DWF to decrease the anthropogenic CO_2 and O_2 in the surface waters, due to vertical mixing and transport to the deepest layers of the basin (Touratier and Goyet, 2011). Similarly, the anticipated Early Pliocene LIW intensification in the Aegean Sea resulting to the strengthening of thermohaline circulation in the area, provides analogous evidence for Mediterranean oxygenation processes in future projections.

Despite the cooling trend and the associated increase of the oxygenation after ~4.6 Ma, as depicted by the trends in the $\delta^{18}O$ and $\delta^{15}N$ profiles, the impact of global cooling events, i.e., Gi20, and the insolation pattern lacking extended maxima, the water column stratification expressed only a slight reduction in the post-4.6 Ma sapropel intervals (see S-index, Fig. 7). This could be explained due to the combined result of LIW enhancement with a simultaneous freshening. Evidence for increased freshwater is suggested by the contemporaneous shift to relatively more negative sapropelic $\delta^{13}C_{org}$ values, still within the marine productivity range, resulting from inputs with a relatively light isotopic signature (Fontugne and Calvert, 1992). Thus, this fresher inflow, which reflects a different source of less saline intrusions to the either way reduced fluvial inputs in between ~4.4–3.9 Ma (Grant et al., 2022), is considered to represent the footprint of the full restoration of the water gateways with the practically isolated North Aegean "Lake Egemar" (Fig. 9b; Krijgsman et al., 2020), as a result of the accelerated rate of Pliocene trench extension in the Cretan Basin (Berniest et al., 2016; Brun et al., 2016). Indeed, the so-called "Lake Egemar", being a mostly Paratethyan-fed brackish water system during the Messinian in the North Aegean, restricted to the south by the Cyclades sill (Fig. 10), was anticipated overspilling to the Mediterranean under the Early Zanclean positive hydrological budget (Krijgsman et al., 2020).

Even though the light $\delta^{13}C_{org}$ values and the elevated CN ARs of deep dwellers *F. profunda*, *Discoaster* spp. and *Helicosphaera* spp. (e.g., in i-cycles 380–390; Figs. 7, 8a) support the presence of DCM and fresh water inputs between ~4.6–3.9 Ma, the striking absence of sapropels 390–380 implies for adequate column ventilation, well defined by the positive shifts in the $\delta^{15}N$ pattern, resulting to the erasure of entire sapropelic cycles.

5.3. Hints on early Pliocene Cretan Basin paleoenvironmental evolution

The available paleogeographic interpretations (e.g., Krijgsman et al., 2020; Andreetto et al., 2021), consider the Cretan Basin to actually represent a shallow epicontinental area during middle Messinian, surrounded by land plateaus, thus forming an isolated basin. The intense opening of the Cretan Sea as a new back-arc basin of the Hellenic arc is related to the extensional post-alpine deformation, with indications that the basin rifting begun in Middle Miocene (e.g., Soukis and Papanikolaou, 2004). Consequently, during Late Miocene-Pliocene, Crete Island should have been moved away from the Cyclades Plateau by a few tens of kilometres (Papanikolaou and Vassilakis, 2010; Papanikolaou, 2021). The extensional regime in the back-arc region, triggered by the south-southwest migration of the trench system and clockwise rotation of the Aegean region, led to a general subsidence and formation of the present-day Aegean Sea. Therefore, the equivalent of the modern Cretan Basin during late Messinian-Pliocene should be a smaller, shallower restricted area, located northern and much closer to Cyclades Plateau (e.g., Le Pichon and Angelier, 1979; Jolivet et al., 2016; ten Veen and Kleinspehn, 2017).

These conditions presumably enabled the deposition of the PLG selenetic gypsum, in water depths not more than 200 m (Roveri et al., 2014). The presence of the overlying vuggy carbonates in the Site 378 record provide additional evidence of subaerial diagenesis (Garrison et al., 1978), suggesting basin's partial desiccation during late Messinian. The complete absence of the rest evaporitic stages as well as the lack of the post-evaporitic "Lago Mare" oligo-mesohaline dolomitic marls (Cita et al., 1990), further support the isolation of the Cretan Basin that prohibited any sediment deposition during the early stages of the MSC event. In contrast, the deeper at that time sites are now days impressively elevated due to the intense tectonic activity, e.g., on land Crete Island, where "Lago Mare" deposits have been documented, unconformably overlying the MSC gypsum (Zachariasse et al., 2011).

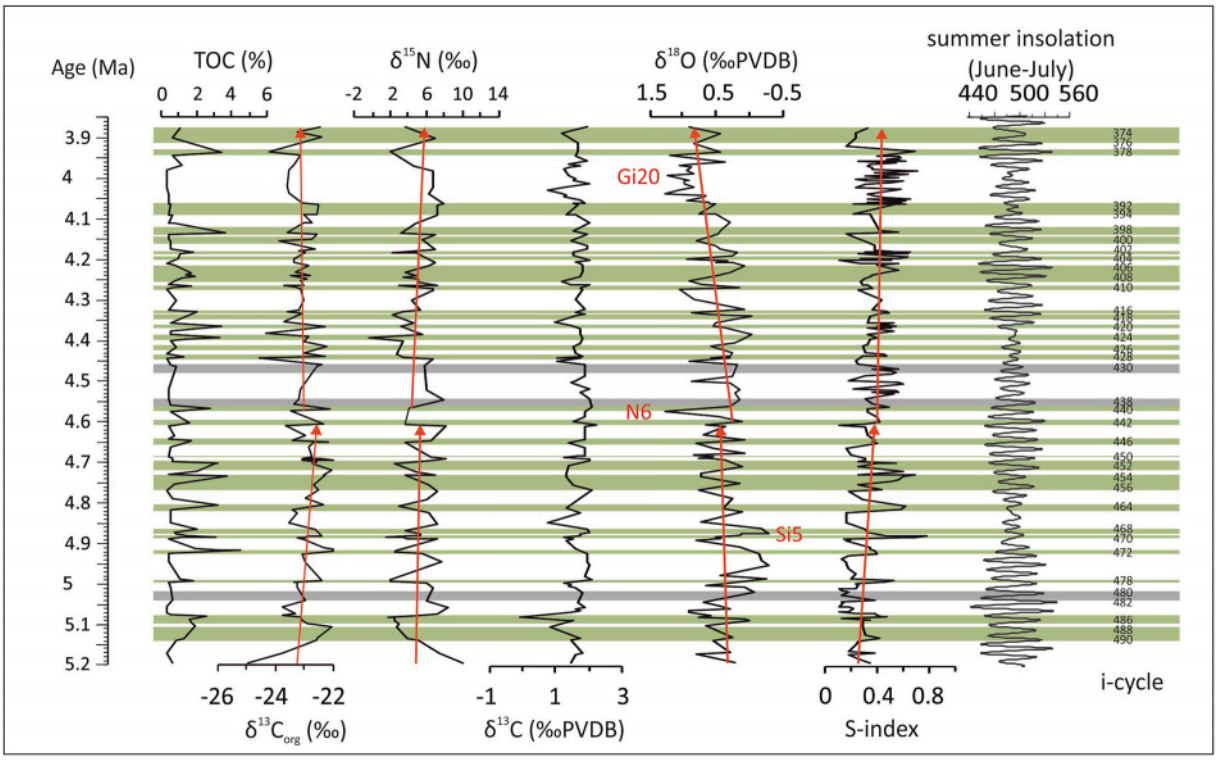

Fig. 7. Site 378 combined dataset of geochemical proxies, S-index and summer isolation pattern (Laskar et al., 2004). Insolation cycles (i-cycles) are after Lourens et al. (1996). Sapropels are highlighted in olive-green bands (according to Hsü et al., 1978) and gray bands (ghost sapropels detected in the present study). Red lines: trendline (linear). (For interpretation of the references to colour in this figure legend, the reader is referred to the web version of this article.)

Our study reveals that the oldest recovered Zanclean marine sediments of pelagic origin with planktonic assemblages and sapropelic interlayers overlying the Messinian selenite PLG paleoenvironments, are dated at 5.195 Ma (Fig. 9a) The estimated stratigraphic hiatus, when assuming the PLG top dated at 5.6 Ma (e.g., Lugli et al., 2010) and the first documented Zanclean sediments at ~5.2 Ma (this study), indicates that the basin remained isolated for at least ~400 kyrs; it's paleogeographic configuration rather prevented any sediment deposition. Hence, provided that the necessary sea level difference should occur, a relatively sudden or gradual restoration of marine conditions in the partially-desiccated Cretan Basin took place, depending on the trends and rhythm of the basin's tectonic evolution. However, the low percentages of benthic foraminiferal assemblage in the early Zanclean deposits (< 20%, Wright, 1978), featured by the dominance of epibathyal taxa, confirm an increase of the approximate deposition paleodepth to at least 500 m (Hsü et al., 1978), supporting the abrupt and relatively sudden change to deep marine environment. In accordance, the estimated low sedimentation values (<~1 cm kyr^{-1}), the well-developed CN assemblages and the prevailing marine origin of the organic matter, reflect open marine sediment accumulation with limited terrestrial input, possibly caused by the opening of the basin in a quite distance from the sediment inflow sources.

Evidently, when considering the modern Aegean Sea bathymetry and land distribution (Fig. 9c) as well as the present study's derived paleoceanographic reconstructions in between ~5.2–4.6 Ma, it is most possible that the main connection between the Cretan Basin and the Mediterraneann Sea till ~4.6 Ma, was restricted mainly to the eastern Aegean region (Fig. 10). The inflow featured by faint LIW masses, mostly occurred through lateral water gateways, such as the Karpathos Straits to the east, although a potential contribution from the Myrtoan Basin to the northwest cannot be excluded. In the subsequent time interval up to ~3.9 Ma, the intensified LIW inflow coupled with "Lake Egemar" less saline intrusions from the North Aegean (Fig. 9b), may have also followed the main pathways from both sides of the Cyclades plateau. Apparently more drilling data from other deep-water Aegean Sea sites (e.g., Krijgsman et al., 2022), are required to confirm the location of the Aegean Sea seawater inflow gateways in the course of the Early Pliocene.

6. Concluding remarks

The CN assemblages together with the geochemical data of DSDP Site 378 in the Cretan Basin, shed new light on the paleoceanographic and paleogeographical evolution of the Early Pliocene sediments consisting of rhythmic alternations of calcareous nannofossil marlstone, ooze and sapropelic interlayers. In brief, our findings are the following:

- CN biostratigraphy and the astronomical calibration of Site 378 sapropel dataset defined the presence of i-cycles 490–374 (~5.2–3.9 Ma). According to the $\delta^{18}O$ and $\delta^{15}N$ isotopic analyses, the sapropelic layers are characterized by warm, low-oxygen conditions.
- Throughout the interval from ~5.2 to 4.6 Ma, the sapropelic layers are characterized by high productivity all over the photic zone, as shown by the high ARs of both *Reticulofenestra* spp. and *F. profunda*; the dominance of the former in the ARs reflects adequate nutrient availability in the surface layers, most possibly associated with relatively increased riverine runoff in the eastern Mediterranean. Thus, the basin remained under the influence of Mediterranean waters with a rather weak LIW inflow.
- In the following ~4.6–3.9 Ma time interval, the increase in the mid-photic zone productivity index *Helicosphaera* spp. and the salinity thriving taxon *U. jafari* within the sapropelic and marly layers respectively, reflects the intensification of the saline and nutrient-enriched LIW presence in the intermediate water depths. Increased intrusion of LIW is expected to reach the Cretan Basin mainly through the marine gateways of Karpathos Straits to the east and possibly the Myrtoan Basin to the northwest. As a result, the presumed alterations of the deep water formation sites between Adriatic

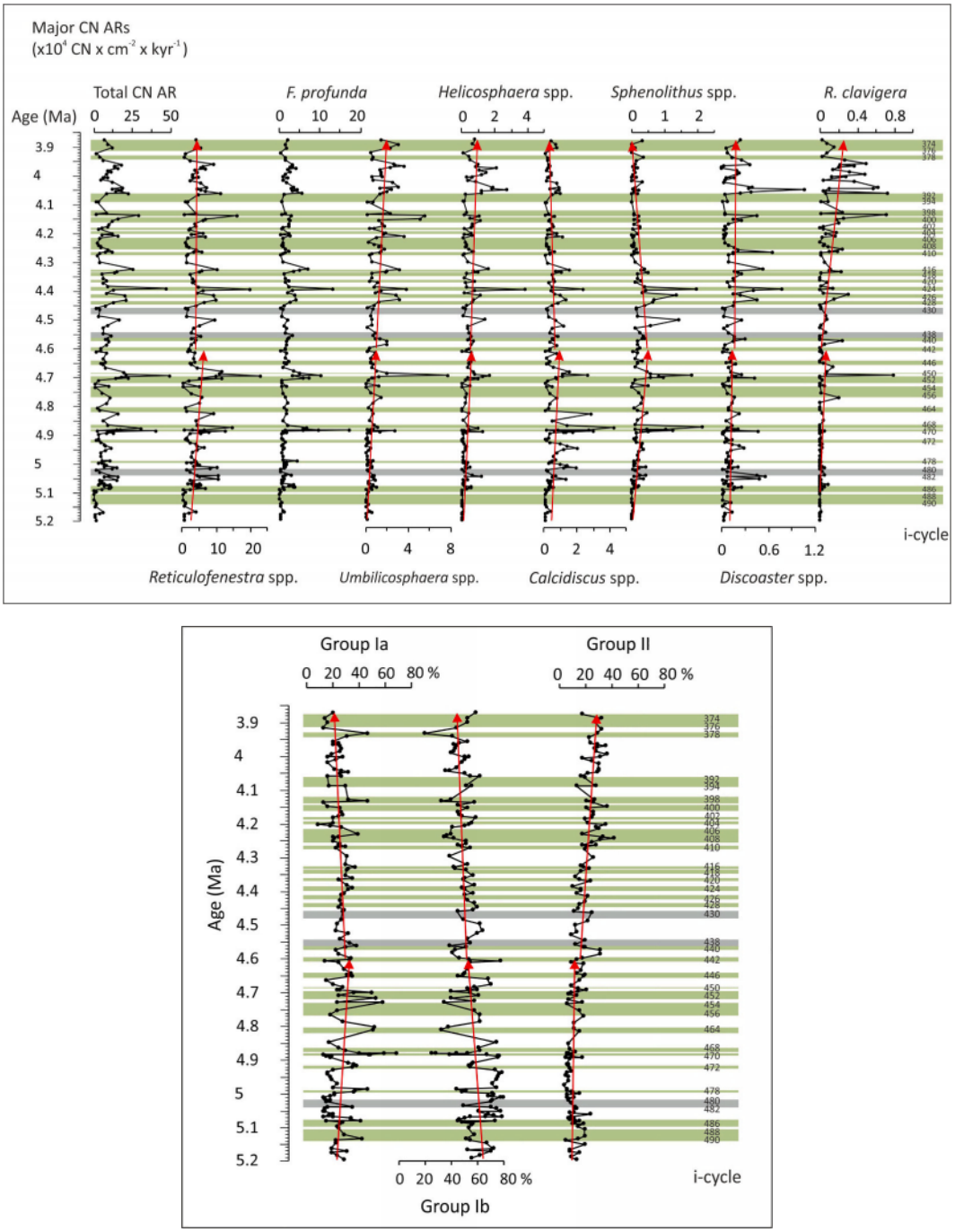

Fig. 8. (a) Site 378 combined dataset: Accumulation Rates of the major calcareous nannofossil species. Red lines: trendline (linear). Sapropels are highlighted in olive-green bands (according to Hsü et al., 1978) and gray bands (ghost sapropels according to the present study). Red lines: trendline (linear). (b) Plot of the produced HCA Groups vs. age (Ma). Sapropels are highlighted in olive-green bands (according to Hsü et al., 1978) and gray bands (ghost sapropels according to the present study). Red lines: trendline (linear). (For interpretation of the references to colour in this figure legend, the reader is referred to the web version of this article.)

and Aegean Seas, similarly to EMT-like phenomena, should have contributed to the area's thermohaline circulation enhancement. The striking absence of sapropels 390–380 implies for adequate column ventilation, well defined by the positive shifts in the $\delta^{15}N$ pattern.

- A simultaneous freshening reflects a different source of less saline intrusions to the either way reduced fluvial inputs in between ~4.4–3.9 Ma, considered to represent the impact of the full restoration of the water gateways with the practically isolated North Aegean "Lake Egemar", as a result of the accelerated rate of Pliocene trench extension in the Cretan Basin.
- The recovery of PLG evaporites from the base of Site 378 and the defined age of the overlying pelagic sediment at ~5.2 Ma indicate that the shallow epicontinental Cretan Basin remained isolated for at least ~400 kyrs after the MSC. The well-developed CN assemblages and the prevailing marine origin of the organic matter combined with the presence of epibathyal benthic foraminifera confirm an increase of the approximate deposition paleodepth to at least 500 m and support a relatively sudden change to deep marine environment in the Cretan Basin during the Early Pliocene.

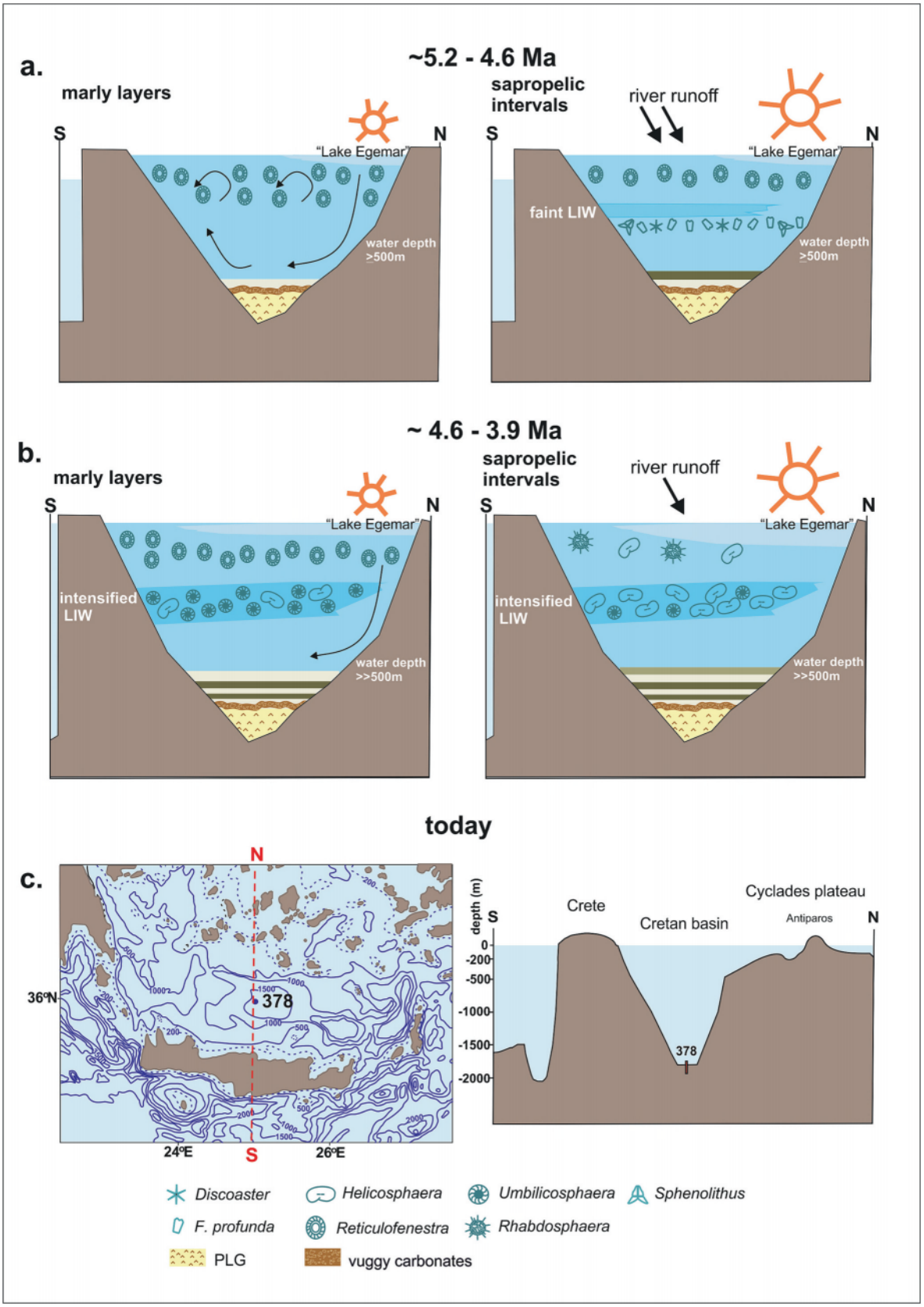

Fig. 9. Cretan Basin schematic cross-sections including the environmental conditions and the dominant calcareous nannofossil assemblages during different time intervals ((a) ~ 5.2–4.6 Ma: reflooded Cretan basin, with faint LIW and Lake Egemar inflows, during the deposition of marly layers (left) and sapropelic intervals (right), (b) ~ 4.6–3.9 Ma: increased LIW and Lake Egemar intrusions with enhanced mid-photic productivity and surface freshening, during the deposition of marly layers (left) and sapropelic intervals (right), (c) Present day geomorphology and cross section (S—N) of the South Aegean Sea.

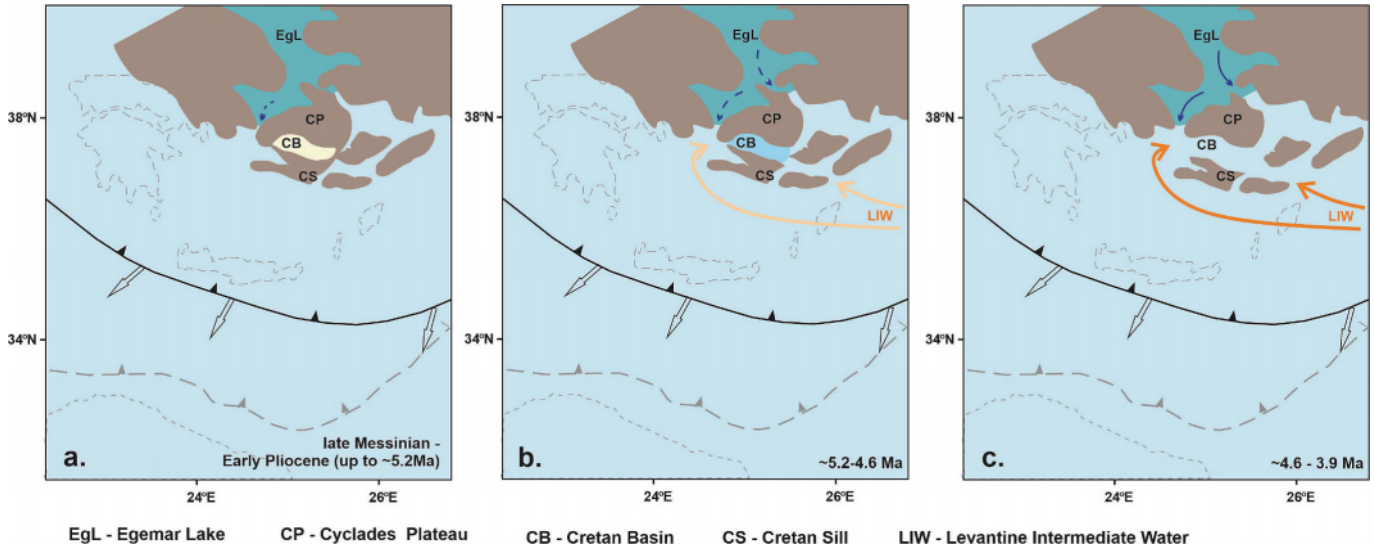

Fig. 10. Sketch map of the South Aegean Sea (a) the desiccated Cretan Basin, (b) ~ 5.2–4.6 Ma: the reflooded Cretan Basin and the major water inflows, (c) ~ 4.6–3.9 Ma: the increased LIW and Lake Egemar intrusions. Ghost lines: present day geographical map; black lines: Pliocene Hellenic forearc and kinematic arrows. Sketch map compilation after van Hinsbergen and van Hinsbergen and Schmid (2012), ten Veen and Kleinspehn (2017); Krijgsman et al. (2020).

CRediT authorship contribution statement

E. Skampa: Conceptualization, Data curation, Writing – original draft, Formal analysis, Funding acquisition. **M.D. Dimiza:** Conceptualization, Writing – original draft, Data curation, Formal analysis, Software. **A. Arabas:** Data curation, Writing – original draft, Funding acquisition, Resources. **A. Gogou:** Formal analysis, Writing – review & editing. **I.P. Panagiotopoulos**: Formal analysis, Writing – review & editing. **Th. Tsourou**: Formal analysis, Writing – review & editing. **D. Velaoras:** Formal analysis, Writing – review & editing. **M. Karagiorgas:** Software. **K.-H. Baumann:** Conceptualization, Formal analysis, Writing – review & editing. **M.V. Triantaphyllou:** Conceptualization, Writing – original draft, Formal analysis, Funding acquisition.

Declaration of competing interest

The authors declare that they have no known competing financial interests or personal relationships that could have appeared to influence the work reported in this paper.

The authors declare the following financial interests/personal relationships which may be considered as potential competing interests:

Elisavet Skampa reports financial support was provided by State Scholarships Foundation. If there are other authors, they declare that they have no known competing financial interests or personal relationships that could have appeared to influence the work reported in this paper.

Data availability

All micropaleontological and geochemical data generated for this study are included in the Supplementary data.

Acknowledgements

This research used samples and data provided by the International Ocean Discovery Program (IODP) and its predecessor programmes for international scientific ocean drilling (DSDP). The sediments obtained from boreholes 378 and 378A are stored in the Integrated Ocean Drilling Project Core Repository at MARUM Bremen E. Skampa has been granted with a scholarship from the State Scholarships Foundation (IKY). This research is co-financed by Greece and the European Union (European Social Fund- ESF) through the Operational Programme «Human Resources Development, Education and Lifelong Learning» in the context of the project "Strengthening Human Resources Research Potential via Doctorate Research – 2nd Cycle" (MIS-5000432), implemented by the State Scholarships Foundation (IKY). We acknowledge support of this work by the IKYDA funding program of the DAAD (project 57260124 "AegeanCocco"), by the Centre National de la Recherche Scientifique (CNRS), CONCLIMA: Constraining large-scale climate feedbacks in the Earth system using paleo data, HORIZON2020, grant number 56.90.13459, by the Greek National Project CLIMPACT: Flagship Initiative for Climate Change and its Impact by the Hellenic Network of Agencies for Climate Impact Mitigation and Adaptation and by the Institute of Geological Sciences and Polish Academy of Sciences for performing the geochemical analysis of the elemental content of sediment samples and analysis of the isotopic composition of carbonates and foraminifera shells.

Appendix A. Supplementary data

Supplementary data to this article can be found online at https://doi.org/10.1016/j.palaeo.2024.112085.

References

Abell, J.T., Winckler, G., Anderson, R.F., Herbert, T.D., 2021. Poleward and weakened westerlies during Pliocene warmth. Nature 589, 70–75. https://doi.org/10.1038/s41586-020-03062-1.

Agnini, C., Monechi, S., Raffi, I., 2017. Calcareous nannofossil biostratigraphy: historical background and application in Cenozoic chronostratigraphy. Lethaia 50, 447–463.

Ali, E., Cramer, W., Carnicer, J., Georgopoulou, E., Hilmi, N.J.M., Le Cozannet, G., Lionello, P., 2022. Cross-Chapter Paper 4: Mediterranean Region. In: Pörtner, H.-O., Roberts, D.C., Tignor, M., Poloczanska, E.S., Mintenbeck, K., Alegría, A., Craig, M., Langsdorf, S., Löschke, S., Möller, V., Okem, A., Rama, B. (Eds.), Climate Change 2022: Impacts, Adaptation and Vulnerability. Contribution of Working Group II to the Sixth Assessment Report of the Intergovernmental Panel on Climate Change. Cambridge University Press, Cambridge, UK and New York, NY, USA, pp. 2233–2272. https://doi.org/10.1017/9781009325844.021.

Amarathunga, U., Hogg, A.M., Rohling, E.J., Roberts, A.P., Grant, K.M., Heslop, D., Hu, P., Liebr, D., Westerhold, T., Zhao, X., Gilmore, S., 2022. Sill-controlled salinity contrasts followed post-Messinian flooding of the Mediterranean. Nat. Geosci. 15 (9), 720–725.

Andreetto, F., Aloisi, G., Raad, F., Heida, H., Flecker, R., Agiadi, K., Lofi, J., Blondel, S., Bulian, F., Camerlenghi, A., 2021. Freshening of the Mediterranean Salt Giant: controversies and certainties around the terminal (Upper Gypsum and Lago-Mare) phases of the Messinian Salinity Crisis. Earth Sci. Rev. 216, 103577 https://doi.org/10.1016/j.earscirev.2021.103577.

Andreetto, F., Flecker, R., Aloisi, G., Mancini, A.M., Guibourdenche, L., de Villiers, S., Krijgsman, W., 2022. High-amplitude water-level fluctuations at the end of the Mediterranean Messinian Salinity Crisis: implications for gypsum formation, connectivity & global climate. EPSL 595, 117767.
Andruleit, H.A., 1996. A filtration technique for quantitative studies of coccoliths. Micropaleontology 42 (4), 403–406.
Arnaboldi, M., Meyers, P.A., 2006. Patterns of carbon and nitrogen stable isotopic compositions of latest Pliocene sapropels from six locations across the Mediterranean. Palaeogeogr. Palaeoclimatol. Palaeoecol. 235, 149–167.
Athanasiou, M., Triantaphyllou, M.V., Dimiza, M.D., Gogou, A., Theodorou, G., 2015. Zanclean/Piacenzian transition on Cyprus (SE Mediterranean): calcareous nannofossil evidence of sapropel formation. Geo-Mar. Lett. 35, 367–385.
Athanasiou, M., Triantaphyllou, M.V., Dimiza, M.D., Gogou, A., Panagiotopoulos, I., Arabas, A., Skampa, E., Kouli, K., Hatzaki, M., Tsiolakis, E., 2021. Reconstruction of oceanographic and environmental conditions in the eastern Mediterranean (Kottafi Hill section, Cyprus Island) during the middle Miocene climate transition. Rev. Micropaleontol. 70, 100480 https://doi.org/10.1016/j.revmic.2020.100480.
Athanasiou, M., Bouloubassi, I., Gogou, A., Klein, V., Dimiza, M.D., Parinos, C., Skampa, E., Triantaphyllou, M.V., 2017. Sea surface temperatures and environmental conditions during the "warm Pliocene" interval (~4.1–3.2Ma) in the Eastern Mediterranean (Cyprus). Glob. Planet. Chang. 2553. https://doi.org/10.1016/j.gloplacha.2017.01.008.
Backman, J., Raffi, I., Rio, D., Fornaciari, E., Pälike, H., 2012. Biozonation and biochronology of Miocene through Pleistocene calcareous nannofossils from low and middle latitudes. Newslett. Strat. 45, 221–244.
Baumann, K.-H., Vollmar, N.M., 2022. Coccolithophore response to changes in surface water conditions south of Iceland (ODP Site 984) between 130 and 56 ka. Mar. Micropaleontol. 175, 102149 https://doi.org/10.1016/j.marmicro.2022.102149.
Baumann, K.-H., Andruleit, H.A., Su, X., 1998. Comparison of different preparation techniques for quantitative nannofossil studies. J. Nannoplankton Res. 20 (2), 75–80.
Baumann, K.-H., Saavedra-Pellitero, M., Böckel, B., Ott, C., 2016. Morphometry, biogeography and ecology of Calcidiscus and Umbilicosphaera in the South Atlantic. Rev. Micropaleontol. 59 (3), 239–251. https://doi.org/10.1016/j.revmic.2016.03.001.
Beltran, C., Flores, J.A., Sicre, M.A., Baudin, F., Renard, M., de Rafélis, M., 2011. Long chain alkenones in the early Pliocene Sicilian sediments (Trubi Formation-Punta di Maiata section): implications for the alkenone paleothermometry. Palaeogeogr. Palaeoclimatol. Palaeoecol. 308, 253–263. https://doi.org/10.1016/j.palaeo.2011.03. 017.
Berniest, A., Brun, J.P., Gorini, C., Crombez, V., Deschamps, R., Hamon, Y., Smit, J., 2016. Interaction between trench retreat and Anatolian escape as recorded by neogene basins in the northern Aegean Sea. Mar. Pet. Geol. 77, 30–42. https://doi.org/10.1016/j.marpetgeo.2016.05.011.
Blanc, P.L., 2002. The opening of the Plio-Quaternary Gibraltar Strait: assessing the size of a cataclysm. Geodin. Acta 15 (5/6), 303–317.
Bornemann, A., Aschwer, U., Mutterlose, J., 2003. The impact of calcareous nannofossils on the pelagic carbonate accumulation across the Jurassic/cretaceous boundary. Palaeogeogr. Palaeoclimatol. Palaeoecol. 199, 187–228. https://doi.org/10.1016/S0031-0182(03)00507-8.
Bouloubassi, I., Rullkötter, J., Meyers, P.A., 1999. Origin and transformation of organic matter in Pliocene–Pleistocene Mediterranean sapropels: organic geochemical evidence reviewed. Mar. Geol. 153, 177–197.
Bowman, C.L., Rand, D.S., Lisiecki, L.E., Bova, S.C., 2023. An 800-kyr planktonic δ 18 O stack for the West Pacific warm Pool. Earth Syst. Sci. Data Discuss. 2023, 1–19. https://doi.org/10.5194/essd-2023-335.
Brun, J.-P., Faccenna, C., Gueydan, F., Sokoutis, D., Philippon, M., Kydonakis, K., Gorini, C., 2016. The two-stage Aegean extension, from localized to distributed, a result of slab rollback acceleration. Can. J. Earth Sci. 53 (11), 1142–1157.
Cacho, I., Grimalt, J.O., Canals, M., Sbaffi, L., Shackleton, N.J., Schönfeld, J., Zahn, R., 2001. Variability of the western Mediterranean Sea surface temperature during the last 25,000 years and its connection with the Northern Hemisphere climatic changes. Paleoceanogr. 16, 40–52.
Capotondi, L., Soroldoni, E., Principato, M.S., Corselli, C., 2002. Late Quaternary planktonic foraminiferal distributions: Problems related to size fraction. In Proceedings of the first Italian meeting on Environmental Micropaleontology, Urbino, Italy, 4–6 June 2002. In: Coccioni, R.G.S., Lirer, F. (Eds.), Grzybowski Foundation, vol. 2004, 9. Special Publication, Krakow, Poland, pp. 1–6.
Carnevale, G., Schwarzhans, W., 2022. Marine life in the Mediterranean during the Messinian salinity crisis: a paleoichthyological perspective. Riv. Ital. Paleontol. Stratigr. 128 (2), 283–324.
Carnevale, G., Landini, W., Sarti, G., 2006. Mare versus Lago-mare: marine fishes and the Mediterranean environment at the end of the Messinian Salinity Crisis. J. Geol. Soc. Lond. 163 (1), 75–80.
Carnevale, G., Gennari, R., Lozar, F., Natalicchio, M., Pellegrino, L., Dela Pierre, F., 2019. Living in a deep desiccated Mediterranean Sea: an overview of the Italian fossil record of the Messinian salinity crisis. Boll. Soc. Paleontol. Ital. 58, 109–140. https://doi.org/10.4435/BSPI.2019.04.
Caruso, A., Blanc-Valleron, M.-M., Da Prato, S., Pierre, C., Rouchy, J.M., 2020. The late Messinian "Lago-Mare" event and the Zanclean Reflooding in the Mediterranean Sea: New insights from the Cuevas del Almanzora section (Vera Basin, South-Eastern Spain). Earth Sci. Rev. 200, 102993 https://doi.org/10.1016/j.earscirev.2019.102993.
Castradori, D., 1998. Calcareous nannofossils in the basal Zanclean of the eastern Mediterranean Sea: remarks on paleoceanography and sapropel formation. Proc. Ocean Drill. Program Sci. Results 160, 113–123.
Cavaleiro, C., Voelker, A.H.L., Stoll, H., Baumann, K.H., Kulhanek, D.K., Naafs, B.D.A., Stein, R., Grützner, J., Ventura, C., Kucera, M., 2018. Insolation forcing of coccolithophore productivity in the North Atlantic during the middle pleistocene. Quat. Sci. Rev. 191, 318–336. https://doi.org/10.1016/j.quascirev.2018.05.027.
Chaikalis, S., Parinos, C., Möbius, J., Gogou, A., Velaoras, D., Hainbucher, D., Sofianos, S., Tanhua, T., Cardin, V., Proestakis, E., Amiridis, V., Androni, A., Karageorgis, A., 2021. Optical properties and biochemical indices of marine particles in the open Mediterranean Sea: The R/V Maria S. Merian Cruise, March 2018. Front. Earth Sci. 9, 614703. https://doi.org/10.3389/feart.2021.614703.
Cita, M.B., Santambrogio, S., Melillo, B., Rogate, F., 1990. Messinian paleoenvironments: New evidence from the Tyrrhenian Sea (ODP Leg 107). In: Kastens, K.A., Mascle, J. (Eds.), Proceedings of the Ocean Drilling Program, Scientific Results, vol. 107, pp. 211–227.
Colin, C., Duhamel, M., Siani, G., Dubois-Dauphin, Q., Ducassou, E., Liu, Z., et al., 2021. Changes in the intermediate water masses of the Mediterranean Sea during the last climatic cycle—New constraints from Neodymium isotopes in foraminifera. Paleoceanogr. Paleoclimatol. 36 (4) https://doi.org/10.1029/2020PA004153 e2020PA004153.
Corbí, H., Soria, J.M., Lancis, C., Giannetti, A., Tent-Manclús, J.E., Dinarès-Turell, J., 2016. Sedimentological and paleoenvironmental scenario before, during, and after the Messinian Salinity Crisis: the San Miguel de Salinas composite section (western Mediterranean). Mar. Geol. 379, 246–266. https://doi.org/10.1016/j.margeo.2016.05.017.
Corselli, C., Principato, M.S., Maffioli, P., Crudelli, D., 2002. Changes in planktonic assemblages during sapropel S5 deposition: evidence from Urania Basin area, eastern Mediterranean. Paleoceanogr. 17 https://doi.org/10.1029/2000PA000536.
Di Stefano, A., Sturiale, G., 2010. Refinements of calcareous nannofossil biostratigraphy at the Miocene/Pliocene Boundary in the Mediterranean region. Geobios 43 (1), 5–20.
Di Stefano, A., Baldassini, N., Alberico, I., 2015. Surface-water conditions in the Mediterranean Basin during earliest Pliocene as revealed by calcareous nannofossil assemblages: comparison between western and eastern sectors. Palaeogeogr. Palaeoclimatol. Palaeoecol. 440, 283–296.
Dowsett, H., Robinson, M., Haywood, A., Salzmann, U., Hill, D., Sohl, L., Chandler, M., Williams, M., Foley, K., Stoll, D., 2010. The PRISM3D paleoenvironmental reconstruction. Stratigraphy 7, 123–139.
Dowsett, H., Dolan, A., Rowley, D., Moucha, R., Forte, A.M., Mitrovica, J.X., Pound, M., Salzmann, U., Robinson, M., Chandler, M., Foley, K., Haywood, A., 2016. The PRISM4 (mid-Piacenzian) paleoenvironmental reconstruction. Clim. Past 12, 1519–1538. https://doi.org/10.5194/cp-12-1519-2016.
Fedorov, A.V., Brierley, C.M., Lawrence, K.T., Liu, Z., Dekens, P.S., Ravelo, A.C., 2013. Patterns and mechanisms of early Pliocene warmth. Nature 496, 43–49.
Fischer, A.G., Hilgen, F.J., Garrison, R.E., 2009. Mediterranean contributions to cyclostratigraphy and astrochronology. Sedimentology 56, 63–94. https://doi.org/10.1111/j.1365-3091.2008.01011.
Flores, J.A., Bárcena, M.A., Sierro, F.J., 2000. Ocean-surface and wind dynamics in the Atlantic Ocean off Northwest Africa during the last 140,000 years. Palaeogeogr. Palaeoclimatol. Palaeoecol. 161, 459–478.
Flores, J.A., Sierro, F.J., Filippelli, G.M., Bárcena, M.A., Pérez-Folgado, M., Vázquez, A., Utrilla, R., 2005. Surface water dynamics and phytoplankton communities during deposition of cyclic late Messinian sapropel sequences in the western Mediterranean. Mar. Micropaleontol. 56, 50–79.
Fontugne, M.R., Calvert, S.E., 1992. Late Pleistocene variability of the carbon isotopic composition of organic matter in the eastern Mediterranean: monitor of changes in carbon sources and atmospheric CO2 concentrations. Paleoceanography 7, 1–20.
Gačić, M., Schroeder, K., Civitarese, G., Vetrano, A., Eusebi Borzelli, G.L., 2012. On the relationship among the Adriatic–Ionian Bimodal Oscillating System (BiOS), the Eastern Mediterranean salinity variations and the Western Mediterranean thermohaline cell. Ocean Sci. Discuss. 9, 2561–2580. https://doi.org/10.5194/osd-9-2561-2012.
Garcia-Castellanos, D., Estrada, F., Jiménez-Munt, I., et al., 2009. Catastrophic flood of the Mediterranean after the Messinian salinity crisis. Nature 462, 778–781. https://doi.org/10.1038/nature08555.
Garcia-Castellanos, D., Micallef, A., Estrada, F., Camerlenghi, A., Ercilla, G., Periáñez, R., Abril, J.M., 2020. The Zanclean megaflood of the Mediterranean–Searching for independent evidence. Earth Sci. Rev. 201, 103061.
Garrison, R., Schreiber, B.C., Bernouilli, D., Fabricius, F., Kidd, R., Mélières, F., 1978. Sedimentary petrology and structures of Mediterranean evaporitic sediments in the Mediterranean Sea. In: Hsü, K.J., Montadert, L., et al. (Eds.), Initial Rep. Deep Sea Drill. Proj., 42A. US Government Printing Office, Washington, DC, pp. 571–612.
Georgopoulos, D., Theocharis, A., Zodiatis, G., 1989. Intermediate water formation in the Cretan Sea (South Aegean Sea). Oceanol. Acta 12 (4), 353–359.
Georgopoulos, D., Chronis, G., Zervakis, V., Lykousis, V., Poulos, S., Iona, A., 2000. Hydrology and circulation in the Southern Cretan Sea during the CINCS experiment (May 1994-September 1995). Prog. Oceanogr. 46, 85–112.
Geraga, M., Ioakim, C., Papatheodorou, G., Ferentinos, G., 2000. Evaluation of palaeoenvironmental changes during the last 18,000 years in the Myrtoon basin. Palaeogeogr Palaeoclimatol Palaeoecol 156 (1–2), 1–17.
Geraga, M., Tsaila-Monopolis, S., Ioakim, C., Papatheodorou, G., Ferentinos, G., 2005. Short-term climate changes in the southern Aegean Sea over the last 48,000 years. Palaeogeogr. Palaeoclimatol. Palaeoecol. 220 (3–4), 311–332.
Gogou, A., Bouloubassi, I., Lykousis, V., Arnaboldi, M., Gaitani, P., Meyers, P.A., 2007. Organic geochemical evidence of late Glacial-Holocene climate instability in the North Aegean Sea. Palaeogeogr. Palaeoclimatol. Palaeoecol. 256, 1–20.
González-Lanchas, A., Hernandez-Almeida, I., Flores, J.-A., Sierro, F.J., Guitian, J., Stoll, H.M., 2021. Carbon isotopic fractionation of alkenones and Gephyrocapsa

coccoliths over the late Quaternary (marine isotope stages 12–9) glacial-interglacial cycles at the western tropical Atlantic. Paleoceanogr. Paleoclimatol. 36 https://doi.org/10.1029/2020PA004175 e2020PA004175.
Gradstein, F.M., Ogg, J.G., 2020. Chapter 2 - the Chronostratigraphic Scale. Geol. Time Scale. 1, 21–32. https://doi.org/10.1016/B978-0-12-824360-2.00002-4.
Grant, K.M., Amarathunga, U., Amies, J.D., et al., 2022. Organic carbon burial in Mediterranean sapropels intensified during Green Sahara periods since 3.2 Myr ago. Commun Earth Environ 3, 11. https://doi.org/10.1038/s43247-021-00339-9.
Grelaud, M., Marino, G., Ziveri, P., Rohling, E.J., 2012. Abrupt shoaling of the nutricline in response to massive freshwater flooding at the onset of the last interglacial sapropel event. Paleoceanography 27, PA3208. https://doi.org/10.1029/2012PA002288.
Haywood, A.M., Valdes, P.J., 2004. Modeling Pliocene warmth: contribution of atmosphere, oceans and cryosphere. EPSL 218, 363–377.
Haywood, A.M., Sellwood, B.W., Valdes, P.J., 2000. Regional warming: Pliocene (3 Ma) paleoclimate of Europe and the Mediterranean. Geology 28, 1063–1066.
Hernández-Almeida, I., Ausín, B., Saavedra-Pellitero, M., Baumann, K.-H., Stoll, H.M., 2019. Quantitative reconstruction of primary productivity in low latitudes during the last glacial maximum and the mid-to-late Holocene from a global Florisphaera profunda calibration dataset. Quat. Sci. Rev. 205, 166–181. https://doi.org/10.1016/j.quascirev.2018.12.016.
Higgins, M.B., Robinson, R.S., Carter, S.J., Pearson, A., 2010. Evidence from chlorin nitrogen isotopes for alternating nutrient regimes in the eastern Mediterranean Sea. Earth Planet. Sci. Lett. 290, 102–107.
Hilgen, F.J., 1987. Sedimentary rhythms and high-resolution chronostratigraphic correlations in the Mediterranean Pliocene. Newsl. Stratigr. 17, 109–127.
Hilgen, F.J., 1991. Astronomical calibration of Gauss to Matuyama sapropels in the Mediterranean and implication for the geomagnetic polarity time scale. Earth Planet. Sci. Lett. 104, 226–244.
van Hinsbergen, D.J.J., Schmid, S.M., 2012. Map-view restoration of Aegean-west Anatolian accretion and extension since the Eocene. Tectonics 31, TC5005.
Hsü, K.J., Montadert, L., Bernoulli, D., Cita, M.B., Erikson, A., Garrison, R.E., Kidd, R.B., Melieres, F., Muller, C., Wright, R.H., 1978. Initial Report of Deep Sea Drilling Project. Mediterranean Sea, 42. U.S. Government Printing Office, Washington, DC.
Iaccarino, S., Bossio, A., 1999. Paleoenvironment of uppermost Messinian sequences in the western Mediterranean (Sites 974, 975,and 978). In: Proceedings of the Ocean Drilling Program, Scientific Results, Vol. 161. Ocean Drilling Program, College Station, TX, pp. 529–541.
Incarbona, A., Ziveri, P., Sabatino, N., Salvagio Manta, D., Sprovieri, M., 2011. Conflicting coccolithophore and geochemical evidence for productivity levels in the Eastern Mediterranean sapropel S1. Mar. Micropaleontol. 81, 3–4, 131–143. ISSN 0377-8398,. https://doi.org/10.1016/j.marmicro.2011.09.003.
Jolivet, L., Goffé, B., Monié, P., Truffert-Luxey, C., Patriat, M., Bonneau, M., 1996. Miocene detachment in Crete and exhumation P-T-t paths of high pressure metamorphic rocks. Tectonics 15, 1129–1153.
Jolivet, L., Augier, R., Robin, C., Suc, J.-P., Rouchy, J.M., 2016. Lithospheric-scale geodynamic context of the Messinian salinity crisis. Sediment. Geol. 188–189, 9–33.
Karakitsios, V., Roveri, M., Lugli, S., Manzi, V., Gennari, R., Antonarakou, A., Triantaphyllou, M., Agiadi, K., Kontakiotis, G., 2013. Remarks on the Messinian evaporites of Zakynthos Island (Ionian Sea, eastern Mediterranean). Bull. Geol. Soc. Greece 47.
Karakitsios, V., Roveri, M., Lugli, S., Manzi, V., Gennari, R., Antonarakou, A., Triantaphyllou, M., Agiadi, K., Kontakiotis, G., Kafousia, N., de Rafelis, M., 2017. A record of the Messinian salinity crisis in the eastern Ionian tectonically active domain (Greece, eastern Mediterranean). Basin Res. 29, 203–233. https://doi.org/10.1111/bre.12173.
Katsouras, G., Gogou, A., Bouloubassi, I., Emeis, K.C., Triantaphyllou, M., Roussakis, G., Lykousis, V., 2010. Organic carbon distribution and isotopic composition in three records from the eastern Mediterranean Sea during the Holocene. Org. Geochem. 41, 935–939.
Kidd, R.B., Cita, M.B., Ryan, W.B.F., 1978. Stratigraphy of eastern Mediterranean sapropel sequences recovered during Leg 42A and their paleoenvironmental significance. Initial Rep. Deep Sea Drill. Proj. 42A, 421–443.
Kotov, S., Paelike, H., 2018. QAnalySeries-a Cross-Platform Time Series Tuning and Analysis Tool. AGU Fall Meeting Abstracts, pp. 53–1230.
Krijgsman, W., Hilgen, F.J., Raffi, I., Sierro, F.J., Wilson, D.S., 1999. Chronology, causes and progression of the Messinian salinity crisis. Nature 400, 652–655.
Krijgsman, W., Palcu, D., Andreetto, F., Stoica, M., Mandic, O., 2020. Changing seas in the late Miocene Northern Aegean: a Paratethyan aroach to Mediterranean basin evolution. Earth Sci. Rev. 103386 https://doi.org/10.1016/j.earscirev.2020.103386.
Krijgsman, W., Vasiliev, I., Beniest, A., Lyons, T., Lofi, J., Tari, G., Slomp, C.P., Cagatay, N., Triantaphyllou, M., Flecker, R., Palcu, D., McHugh, C., Arz, H., Henry, P., Lloyd, K., Cifci, G., Sipahioglu, Ö., Sakellariou, D., the BlackGate workshop participants, 2022. Mediterranean–Black Sea gateway exchange: scientific drilling workshop on the BlackGate project. Sci. Drill. 31, 93–110. https://doi.org/10.5194/sd-31-93-2022.
Lamb, A.L., Wilson, G.P., Leng, M.J., 2006. A review of coastal palaeoclimate and relative sea-level reconstructions using d13 C and C/N ratios in organic material. Earth-Sci. Rev. 75, 29–57.
Langereis, C.G., Hilgen, F.J., 1991. The Rossello composite: a Mediterranean and global reference section for the early to early late Pliocene. EPSL 104, 211–225.
Lascaratos, A., Williams, R.G., Tragou, E., 1993. A Mixed-Layer Study of the Formation of Levantine Intermediate Water. J. Geophys. Res. 98, C8, 14.739–14.749.
Laskar, J., Robutel, P., Joutel, F., Gastineau, M., Correia, A.C.M., Levrard, B., 2004. A long term numerical solution for the insolation quantities of the Earth. Astron. Astrophys. 428, 261–285.
Le Pichon, X., Angelier, J., 1979. The Hellenic Arc and Trench system: a key to the neotectonic evolution of the Eastern Mediterranean area. Tectonophysics 69, l–42.
Lirer, F., Foresi, L.M., Iaccarino, S.M., Salvatorini, G., Turco, E., Cosentino, C., Sierro, F. J., Caruso, A., 2019. Mediterranean Neogene planktonic foraminifer biozonation and biochronology. Earth. Rev. 196, 102869 https://doi.org/10.1016/j.earscirev.2019.05.013.
Lisiecki, L.E., Raymo, M.E., 2005. A Pliocene-Pleistocene stack of 57 globally distributed benthic δ18O records. Paleoceanogr. 20, PA1003.
Lourens, L.J., Hilgen, F.J., Zachariasse, W.J., Van Hoof, A.A.M., Antonarakou, A., Vergnaud-Grazzini, C., 1996. Evaluation of the Pliocene to early Pleistocene astronomical time scale. Paleoceanogr. 11, 391–413.
Lugli, S., Manzi, V., Roveri, M., Schreiber, B.C., 2010. The primary lower Gypsum in the Mediterranean: a newfacies interpretation for the first stage of the Messinian salinity crisis. Palaeogeogr. Palaeoclimatol. Palaeoecol. 297, 83–99.
Lugli, S., Gennari, R., Gvirtzman, Z., Manzi, V., Roveri, M., Schreiber, B.C., 2013. Evidence of clastic evaporites in the canyons of the Levant Basin (Israel): implications for the Messinian Salinity Crisis. J. Sediment. Res. 83, 942–954.
Lykousis, V., Chronis, G., Tselepides, A., Price, N.B., Theocharis, A., Siokou-Fragou, I., Van Wambeke, F., Danovaro, R., Stavrakakis, S., Duineveld, G., Georgopoulos, D., Ignatiades, L., Souvermezoglou, A., Voutsinou-Taliadouri, F., 2002. Major outputs of the recent multidisciplinary biogeochemical researches undertaken in the Aegean Sea. J. Mar. Syst. 33–34, 313–334.
Malinverno, E., Triantaphyllou, M.V., Stavrakakis, S., Ziveri, P., Lykousis, V., 2009. Seasonal and spatial variability of coccolithophore export production at the South-Western margin of Crete (Eastern Mediterranean). Mar. Micropaleontol. 71, 131–147.
Mancini, A.M., Gennari, R., Natalicchio, M., Dela Pierre, F., Carnevale, G., Pastero, L., Pellegrino, L., Pilade, F., Lozar, F., 2022. Taphonomic bias on calcareous micro and nannofossils and paleoenvironmental evolution across the Messinian Salinity Crisis onset: insights from the Sorbas Basin (SE Spain). Palaeogeogr. Palaeoclimatol. Palaeoecol. 111056 https://doi.org/10.1016/j.palaeo.2022.111056.
Mancini, A.M., Bocci, G., Morigi, C., Gennari, R., Lozar, F., Negri, A., 2023. Past analogues of deoxygenation events in the Mediterranean Sea: a tool to constrain future impacts. J. Mar. Sci. Eng. 2023 (11), 562. https://doi.org/10.3390/jmse11030562.
Marsaglia, K.M., Fukusawa, H., Cornell, W.C., Skilbeck, C.G., Meyers, P.A., Prasad, M., Klaus, A., 2004. Eustatic signals in deep-marine sedimentary sequences recovered at ODP Site 978, Alboran Basin, Western Mediterranean Sea. J. Sediment. Res. 74 (3), 379–391.
Martini, E., 1971. Standard tertiary and quaternary calcareous nannoplankton zonation. In: Farinacci, A. (Ed.), Proceedings of the Second Planktonic Conference (Rome) Technoscienza, pp. 739–785.
Mascle, J., Martin, L., 1990. Shallow structure and recent evolution of the Aegean Sea: a synthesis based on continuous reflection profiles. Mar. Geol. 94, 271–299.
Mitchell, R.N., Bice, D.B., Montanari, A., Cleaveland, L., Christianson, K.T., Coccioni, R., Hinnov, L.A., 2008. Oceanic anoxic cycles? Orbital prelude to the Bonarelli Level (OAE2). Earth Planet. Sci. Lett. 267, 1–16.
Möbius, J., Lahajnar, N., Emeis, K.-C., 2010. Diagenetic Control of Nitrogen Isotope Ratios in Holocene Sapropels and recent Sediments from the Eastern Mediterranean Sea. Biogeosciences 7, 3901–3914. https://doi.org/10.5194/bg-7-3901-2010.
Molfino, B., McIntyre, A., 1990. Precessional forcing of nutricline dynamics in the equatorial Atlantic. Science 249, 766–769.
Mourik, A.A., Bijkerk, J.F., Cascella, A., Hüsing, S.K., Hilgen, F.J., Lourens, L.J., Turco, E., 2010. Astronomical tuning of the La Vedova High Cliff section (Ancona, Italy)—Implications of the Middle Miocene climate transition for Mediterranean sapropel formation. Earth Planet. Sci. Lett. 297, 249–261.
Müller, C., 1978. Neogene Calcareous Nannofossils from the Mediterranean—Leg 42A of the Deep Sea Drilling Project. In: Hsu, K.J., Montadert, L., et al. (Eds.), Init. Repts. DSDP, 42: Washington (U.S. Printing Office), pp. 727–751.
Nannotax 3; http://www.mikrotax.org/Nannotax3/.
Nijenhuis, I.A., de Lange, G.J., 2000. Geochemical constraints on Pliocene sapropel formation in the eastern Mediterranean. Mar. Geol. 163, 41–63.
Ochoa, D., Sierro, F.J., Lofi, J., Maillard, A., Flores, J.A., Suárez, M., 2015. Synchronous onset of the Messinian evaporite precipitation: first Mediterranean offshore evidence. Earth Planet. Sci. Lett. 427, 112–124.
Olausson, E., 1961. Studies of deep sea cores. Rep. Swed. Deep-Sea Exped. 1947–1948 (8–6), 336–391.
Palumbo, E., Flores, J.A., Perugia, C., Petrillo, Z., Voelker, A.H.L., Amore, F.O., 2013. Millennial scale coccolithophore paleoproductivity and sur- face water changes between 445 and 360 ka (Marine Isotope Stages 12/11) in the Northeast Atlantic. Palaeogeogr. Palaeoclimatol. Palaeoecol. 383–384, 27–41.
Papanikolaou, D., 2021. The geology of Greece. Reg. Geol. Rev. https://doi.org/10.1007/978-3-030-60731-9. ISBN 978-3-030-60730-2.
Papanikolaou, D., Vassilakis, E., 2010. Thrust faults and extensional detachment faults in Cretan tectono-stratigraphy: implications for Middle Miocene extension. Tectonophysics 488, 233–247.
Parras-Berrocal, I.M., Vazquez, R., Cabos, W., Sein, D.V., Álvarez, O., Bruno, M., Izquierdo, A., 2021. Will deep water formation collapse in the North Western Mediterranean Sea by the end of the 21st century? ESS Open Archive. https://doi.org/10.1002/essoar.10507698.1.
Parras-Berrocal, I.M., Vazquez, R., Cabos, W., Sein, D.V., Álvarez, O., Bruno, M., Izquierdo, A., 2023. Dense water formation in the Eastern Mediterranean under

global warming scenario. EGUsphere [preprint] 2023. https://doi.org/10.5194/egusphere-2023-159.
Pedersen, T.F., Calvert, S.E., 1990. Anoxia vs. productivity: what controls the formation of organic-carbon-rich sediments and sedimentary rocks? AAPG Bull. 74, 454–466.
Pellegrino, L., Natalicchio, M., Abe, K., Jordan, R.W., Longo, S.E.F., Ferrando, S., Carnevale, G., Dela Pierre, F., 2021. Tiny, glassy, and rapidly trapped: the nano-sized planktic diatoms in Messinian (late Miocene) gypsum. Geology 49 (11), 1369–1374. https://doi.org/10.1130/G49342.1.
Pilade, F., Vasiliev, I., Birgel, D., Pierre, F.D., Natalicchio, M., Mancini, A., Carnevale, G., Gennari, R., 2023. Deciphering the termination of the Messinian salinity crisis: the alkenone record of the Miocene-Pliocene transition in the northern Mediterranean. Palaeogeogr. Palaeoclimatol. Palaeoecol. 631, 111831.
Plancq, J., Grossi, V., Pittet, B., Huguet, C., Rosell-Melé, A., Mattioli, E., 2015. Multi-proxy constraints on sapropel formation during the late Pliocene of Central Mediterranean (Southwest Sicily). Earth Planet. Sci. Lett. 420, 30–44.
Popescu, S.M., Melinte, M.C., Suc, J.P., Clauzon, G., Quillévéré, F., Süto-Szentai, M., 2007. Earliest Zanclean age for the Colombacci and uppermost Di Tetto formations of the "latest Messinian" northern Apennines: New paleoenvironmental data from the Maccarone section (Marche Province, Italy). Geobios 40 (3), 359–373. https://doi.org/10.1016/j.geobios.2006.11.005.
Popescu, S.-M., Melinte, M.-C., Suc, J.-P., Clauzon, G., Quillevere, F., Süto-Szentai, M., 2008. Marine reflooding of the Mediterranean after the Messinian Salinity Crisis predates the Zanclean GSSP. Reply to the "Comment on 'Earliest Zanclean age for the Colombacci and uppermost Di Tetto formations of the "latest Messinian" northern Apennines: new paleoenvironmental data from the Maccarone section (Marche Province, Italy)'" by Popescu et al. (2007). Geobios 40 (359–373) authored by Roveri et al. Geobios 41, 657–660.
Principato, M.S., Crudeli, D., Ziveri, P., Slomp, C.P., Corselli, C., Erba, E., de Lange, G.J., 2006. Phyto- and zooplankton paleofluxes during the deposition of sapropel S1 (eastern Mediterranean): Biogenic carbonate preservation and paleoecological implications. Palaeogeogr. Palaeoclimatol. Palaeoecol. 235, 8–27.
Psarra, S., Tselepides, A., Ignatiades, L., 2000. Primary productivity in the oligotrophic Cretan Sea (NE Mediterranean): seasonal and interannual variability. Prog. Oceanogr. 46, 187–204.
Rohling, E.J., Marino, G., Grant, K.M., 2015. Mediterranean climate and oceanography, and the periodic development of anoxic events (sapropels). Earth Sci. Rev. 143, 62–97.
Rossignol-Strick, M., 1983. African monsoons, an immediate climate response to orbital insolation. Nature 304, 46–49.
Rossignol-Strick, M., 1985. Mediterranean Quaternary sapropels, an immediate response of the African Monsoon to variation of insolation. Palaeogeogr. Palaeoclimatol. Palaeoecol. 49, 237–263.
Sediment drifts of the Corsica channel, northern Tyrrhenian Sea. In: Roveri, M., Stow, D. A.V., Faugéres, J.C., Pudsey, C.J., Viana, A.R. (Eds.), 2002. 2002. Deep Water Contourites Systems: Modern Drifts and Ancient Series, Seismic and Sedimentary Characteristics, vol. 22. Geol. Society Memoirs, London, pp. 191–208.
Roveri, M., Bertini, A., Cipollari, P., Cosentino, D., Di Stefano, A., Florindo, F., Gennari, R., Gliozzi, E., Grossi, F., Iaccarino, S., Lugli, S., Manzi, V., 2008. Comment on "Earliest Zanclean age for the Colombacci and uppermost Di Tetto formations of the "latest Messinian" northern Apennines: new palaeoenvironmental data from the Maccarone section (Marche Province, Italy)" by Popescu et al. (2007) Geobios 40 (359–373). Geobios 41, 669–675.
Roveri, M., Flecker, R., Krijgsman, W., Lofi, J., Lugli, S., Manzi, V., Sierro, F.J., Bertini, A., Camerlenghi, A., De Lange, G., Govers, R., Hilgen, F.J., Hubscher, C., Meijer, P.T., Stoica, M., 2014. The Messinian salinity crisis: past and future of a great challenge for marine sciences. Mar. Geol. 352, 25–58. https://doi.org/10.1016/j.margeo.2014.02.002.
Skampa, E., Triantaphyllou, M.V., Dimiza, M.D., Gogou, A., Malinverno, E., Stavrakakis, S., Panagiotopoulos, I.P., Parinos, C., Baumann, K.-H., 2019. Coupling plankton-sediment trap-surface sediment coccolithophore regime in the North Aegean Sea (NE Mediterranean). Mar. Micropaleontol. 152, 101729 https://doi.org/10.1016/j.marmicro.2019.03.001.
Skampa, E., Triantaphyllou, M.V., Dimiza, M.D., Gogou, A., Malinverno, E., Stavrakakis, S., Parinos, C., Panagiotopoulos, I.P., Tselenti, D., Archontikis, O., Baumann, K.-H., 2020. Coccolithophore export in three deep-sea sites of the Aegean and Ionian Seas (Eastern Mediterranean): Biogeographical patterns and biogenic carbonate fluxes. Deep-Sea Res. II Top. Stud. Oceanogr. 171, 104690 https://doi.org/10.1016/j.dsr2.2019.104690.
Soukis, K., Papanikolaou, D., 2004. Contrasting geometry between Alpine and Late- to Post-Alpine tectonic structures in Anafi Island (Cyclades). Bull. Geol. Soc. Greece 36, 1688–1696.
Spezzaferri, S., Cita, M.B., McKenzie, J.A., 1998. The Miocene/Pliocene boundary in the Eastern Mediterranean: results from Sites 967 and 969. In: Proceedings-Ocean Drilling Program Scientific Results (9–28). National Science Foundation.
Stavrakakis, S., Chronis, G., Tselepides, A., Heussner, S., Monaco, A., Abassi, A., 2000. Downward fluxes of settling particles in the deep Cretan Sea (NE Mediterranean). Prog. Oceanogr. 46, 217–240.
Stolz, K., Baumann, K.H., 2010. Changes in palaeoceanography and palaeoecology during Marine Isotope Stage (MIS) 5 in the eastern North Atlantic (ODP Site 980) deduced from calcareous nannoplankton observations. Palaeogeogr. Palaeoclimatol. Palaeoecol. 292, 295–305.
Thunell, R.C., Rio, D., Sprovieri, R., Raffi, J., 1991. Limestone-marl couplets: origin of the early Pliocene Trubi marls in Calabria, Southern Italy. J. Sediment. Petrol. 61, 1109–1122.
Toucanne, S., Jouet, G., Ducassou, E., Bassetti, M.-A., Dennielou, B., Morelle, C., Minto'o, A., Lahmi, M., Touyet, N., Charlier, K., Lericolais, G., Mulder, T., 2012. A 130,000-year record of Levantine Intermediate Water flow variability in the Corsica Trough, western Mediterranean Sea. Quat. Sci. Rev. 33, 55–73. ISSN 0277-3791. https://doi.org/10.1016/j.quascirev.2011.11.020.
Touratier, F., Goyet, C., 2011. Impact of the Eastern Mediterranean Transient on the distribution of anthropogenic CO2 and first estimate of acidification for the Mediterranean Sea. Deep-Sea Res. I 58, 1–15. https://doi.org/10.1016/j.dsr.2010.10.002.
Triantaphyllou, M.V., Ziveri, P., Gogou, A., Marino, G., Lykousis, V., Bouloubassi, I., Emeis, K.C., Kouli, K., Dimiza, M., Rosell-Mele, A., Papanikolaou, M., Katsouras, G., Nunez, N., 2009. Late Glacial-Holocene climate variability at the south-eastern margin of the Aegean Sea. Mar. Geol. 266, 182–197.
Triantaphyllou, M.V., Gogou, A., Dimiza, M.D., Kostopoulou, S., Parinos, K., Rousakis, G., Geraga, M., Bouloubassi, I., Fleitmann, D., Zervakis, V., Velaoras, D., Diamantopoulou, A., Sampatakaki, A., Lykousis, V., 2016. Holocene Climatic Optimum decadal-scale paleoceanography in the NE Aegean (Mediterranean Sea). Geo-Mar. Lett. 31, 51–66.
Tsampouraki-Kraounaki, K., Sakellariou, D., Rousakis, G., Morfis, I., Panagiotopoulos, I., Livanos, I., Manta, K., Paraschos, F., Papatheodorou, G., 2021. The Santorini-Amorgos Shear Zone: evidence for Dextral Transtension in the South Aegean Back-Arc Region, Greece. Geosciences 11, 216. https://doi.org/10.3390/geosciences11050216.
Van Dam, J., 2006. Geographic and temporal patterns in the late Neogene (12–3 Ma) aridification of Europe: the use of small mammals as paleoprecipitation proxies. Palaeogeogr. Palaeoclimatol. Palaeoecol. 238, 190–218.
Vázquez, A., Utrilla, R., Zamarrennō, I., Sierro, F.J., Flores, J.A., Francés, G., 2000. Precession-related sapropels of the Messinian Sorbas Basin (South Spain): paleoenvironmental significance. Palaeogeogr. Palaeoclimatol. Palaeoecol. 158, 353–370.
ten Veen, J.H., Kleinspehn, K.L., 2017. Geodynamics along an increasingly curved convergent plate margin: late Miocene-Pleistocene Rhodes, Greece. Tectonics 21 (3), 1017. https://doi.org/10.1029/2001TC001287.
Velaoras, D., Lascaratos, A., 2010. North–Central Aegean Sea surface and intermediate water masses and their role in triggering the Eastern Mediterranean Transient. J. Mar. Syst. 83, 58–66. https://doi.org/10.1016/j.jmarsys.2010.07.001.
Velaoras, D., Krokos, G., Nittis, K., Theocharis, A., 2014. Dense intermediate water outflow from the Cretan Sea: a salinity driven, recurrent phenomenon, connected to thermohaline circulation changes. J. Geophys. Res. Oceans 119, 4797–4820.
Velaoras, D., Papadopoulos, V.P., Kontoyiannis, H., Papageorgiou, D.K., Pavlidou, A., 2017. The response of the Aegean sea (eastern mediterranean) to the extreme 2016–2017 winter. Geophys. Res. Lett. 44, 9416–9423.
Wade, B.S., Bown, P.R., 2006. Calcareous nannofossils in extreme environments: the Messinian Salinity Crisis, Polemi Basin, Cyprus. Palaeogeogr. Palaeoclimatol. Palaeoecol. 233 (3–4), 271–286.
Wang, P., Tian, J., Lourens, L.J., 2010. Obscuring of long eccentricity cyclicity in Pleistocene oceanic carbon isotope records. Earth Planet. Sci. Lett. 290, 319–330.
Wright, R., 1978. 41. Neogene paleobathymetry of the Mediterranean based on benthic foraminifers from DSDP Leg 42a. Initial Reports DSDP 42, 837–847.
Young, J.R., Bown P.R., Lees J.A. (2022) *Nannotax3 website*. International Nannoplankton Association. Accessed 21 Apr. 2022. URL: www.mikrotax.org/Nannotax3.
Zachariasse, W.J., van Hinsbergen, D.J.J., Rutger Fortuin, A., 2011. Formation and fragmentation of a late Miocene supradetachment basin in Central Crete: implications for exhumation mechanisms of high-pressure rocks in the Aegean forearc. Basin Res. 23 (6), 678–701. https://doi.org/10.1111/j.1365-2117.2011.00507.x.
Zervakis, V., Georgopoulos, D., Karageorgis, A.P., Theocharis, A., 2004. On the response of the Aegean Sea to climatic variability: a review. Int. J. Climatol. 24, 1845–1858.